Lawrence Berkeley National Laboratory
Recent Work

**Title**
REACTION CHANNELS IN THE CAPTURE OF K--MESON BY COMPLEX NUCLEI

**Permalink**
https://escholarship.org/uc/item/6m46447z

**Author**
Patrick, Jack W.

**Publication Date**
1966-03-01

eScholarship.org Powered by the California Digital Library
University of California

UCRL-16602

# University of California
# Ernest O. Lawrence Radiation Laboratory

REACTION CHANNELS IN THE CAPTURE OF
K⁻ MESONS BY COMPLEX NUCLEI

TWO-WEEK LOAN COPY

*This is a Library Circulating Copy which may be borrowed for two weeks. For a personal retention copy, call Tech. Info. Division, Ext. 5545*

Berkeley, California

## DISCLAIMER

This document was prepared as an account of work sponsored by the United States Government. While this document is believed to contain correct information, neither the United States Government nor any agency thereof, nor the Regents of the University of California, nor any of their employees, makes any warranty, express or implied, or assumes any legal responsibility for the accuracy, completeness, or usefulness of any information, apparatus, product, or process disclosed, or represents that its use would not infringe privately owned rights. Reference herein to any specific commercial product, process, or service by its trade name, trademark, manufacturer, or otherwise, does not necessarily constitute or imply its endorsement, recommendation, or favoring by the United States Government or any agency thereof, or the Regents of the University of California. The views and opinions of authors expressed herein do not necessarily state or reflect those of the United States Government or any agency thereof or the Regents of the University of California.

Special Thesis

UCRL-16602

UNIVERSITY OF CALIFORNIA

Lawrence Radiation Laboratory
Berkeley, California

Contract No. W-7405-eng-48

# REACTION CHANNELS IN THE CAPTURE OF $K^-$-MESONS BY COMPLEX NUCLEI

Jack W. Patrick

Ph.D. Thesis

March 1, 1966

REACTION CHANNELS IN THE CAPTURE OF $K^-$-MESONS BY COMPLEX NUCLEI

CONTENTS

ABSTRACT

A total of 13 600 $K^-$-mesons at rest has been observed in two nuclear emulsion stacks. The emission of hyperons, pions, and hyperfragments from 3900 of the $K^-$-capture stars has been studied extensively. The identification of the hyperons is discussed. Charged Σ-hyperons are emitted from (17.3 ± 1.2) percent of all $K^-$-stars in the completely analyzed stack from which the figures following are quoted. The $\Sigma^+/\Sigma^-$ ratio for all stars is 1.08 ± 0.08, while the proportion of stars from which pions are emitted is 0.38 ± 0.05. About 11 percent of all identified charged Σ-hyperons had an energy above 60 MeV, and were therefore attributed to multinucleon reaction channels. The proportion of all multinucleon primary reaction processes may be as high as 46 percent. A detailed examination of the pion-emitting events and of the sign ratio of the mesons has led to an estimate of the probabilities of absorption of Σ-hyperons in the parent nucleus, and to a partition of events between the various single-nucleon reaction channels. On the basis of the Coulomb barrier and Auger electron emission, discrimination is made between $K^-$-capture on light (C,N,O) nuclei and on heavy nuclei (Ag, Br). For the single-nucleon reaction channels it is found that $K^-$-capture by a light nucleus is 1.16 times as likely to produce a pion as a $K^-$-capture by a heavy nucleus. For the multinucleon channels, it is determined that $K^-$-interaction with a light nucleus is 2.36 times as likely to produce a fast ($T_\Sigma > 60$ MeV) Σ-hyperon as interaction with a heavy nucleus. The mechanism of light ($Z < 7$) hyperfragment formation, excluding cryptofragments, is shown by analysis

of the pion spectra accompanying the hypernuclear prong to be primarily one of Σ-conversion (80 percent). A study of the relative number of captures on light and on heavy nuclei yielded the result that less than 20 percent of the production of these light hyperfragments took place on heavy nuclei. Further, a limit of 30 percent was placed on the fraction of light hyperfragments produced in multinucleon reactions. Evidence for the $Y_o^*$ (1405) is studied with $\Sigma\pi$ mass spectra from $K^-$-interactions on $C^{12}$. The results can be explained on an impulse model without recourse to resonance formation. Production of $Y_o^*$ with a width of $< 20$ MeV is not confirmed.

# I. INTRODUCTION

## A. Historical Background

Observations of negative K-mesons were first reported in 1953[1] from nuclear emulsion studies of cosmic radiation. The weak flux of negative K-mesons in such radiation hampered the early studies.[2] This difficulty was partially overcome by the development at both Brookhaven and LRL of machine-produced negative K-meson beams. The relatively low intensities remained a factor limiting investigations.[3,4] At this laboratory the Barkas Group[5] was able to obtain a beam enriched in negative K-mesons by using particles produced in the forward direction and emerging from the bevatron radially after bending in the bevatron field. These passed through a combination of quadrupole magnets, a hydrocarbon energy degrader and then an additional analyzing magnet which performed the necessary mass-separation,

The whole path to the emulsion stack was only the order of one K-meson lifetime, so that even with bevatron beams of only $10^9$ - $10^{10}$ protons per pulse, reasonably good exposures could be made with short running times. Contamination of the K-mesons by electrons and muons remained a problem, but not an insoluble one for emulsion detection. Many emulsion stacks were exposed to this beam, and much analysis, particularly in Europe, of $K^-$-interactions with complex nuclei were carried out.

With the advent of bevatron beams of higher intensity, more selection conditions could be put on the beam, and the development by Murray[6] of the coaxial static-electro-magnetic velocity spectrometer enabled him to obtain a greatly purified negative K-meson beam. The

apparatus employed crossed electric and magnetic fields within coaxial cylindrical conductors to focus desired particles at the exit collimator and deflect undesired ones out of the beam. The beam was refined in this way by a factor of about $10^3$. Later, parallel plate spectrometers operated in tandem produced even purer beams.

The availability of artificially produced negative K-meson beams with such greatly reduced contamination made possible the compilation of statistically significant data on the K-interactions with protons in the hydrogen bubble chamber. A study of the basic process of interaction between the negative K-meson and the nucleon was begun at this time at this laboratory using a 10-inch hydrogen bubble chamber.[7] The analysis of data from these and similar experiments done elsewhere has been the subject of numerous reports and papers,[8-15] which are referred to here. They also contain extensive bibliographies.

The properties of K-mesons were discussed in some detail in early review works by Franzinetti and Morpurgo[8] and by Dalitz[9].

A concentrated experimental effort, known as the $K^-$-collaboration[10], made at that time on the part of several European universities, produced an extensive analysis of negative K-meson interaction with the complex nuclei of photographic emulsions.

In more recent times Morpurgo[12] has reviewed the large amount of work done in the intervening years in the general field of strongly interacting hyperons and heavy mesons. A contemporary article by Burhop et. al.[13] presents a summary of the current situation in processes occurring when the negative K-meson's basic interaction is

viewed as taking place on nuclei, rather than on a single nucleon.

Most recently Sakitt et. al.[15] have studied the low-energy $K^-$-meson interactions in hydrogen and fitted the data to the zero-effective range theory of Dalitz and Tuan[16].

In the present work are presented results obtained from a study of 13 000 $K^-$-interaction stars found in two stacks of improved Ilford K.5 nuclear research emulsion which had been exposed to the purified $K^-$-beam from the bevatron. The $K^-$'s were brought to rest in the central part of the stacks, the dimensions of which were large enough to permit a high percentage of secondary particles to stop in the emulsion. All secondaries were followed out until they came to rest, interacted, decayed, or left the stack. Automated equipment was used where possible to reduce some of the drudgery and improve the accuracy of the measurements. In the subsequent re-analysis of the data, the latest available information on the resonances and the $K^-$-interactions in hydrogen and in deuterium has been used.

The reaction channels of the $K^-$ meson have been investigated for the cases of interaction with a single nucleon and with two nucleons. The role played by resonances in the $K^-$ meson interaction has been studied, as well as the mechanism of hyperfragment production.

B. Basic Interactions

Negative K-mesons which come to rest in nuclear emulsions are captured by the constituent atoms: ejection of an orbital electron is the initial basic capture process. The meson is assumed captured by the atom in a Bohr orbit with very high principle quantum number n. The object formed after capture, a mesic atom, is unstable. The meson

makes transitions into lower orbits by Auger-electron and x-ray emission until it is captured by the nucleus.

The nuclear process, which is the topic of this dissertation, is best approached by consideration of the possible elementary $K^-$-nucleon reactions.

Excluded are the elastic scattering processes:

(a) $K^- + p \rightarrow K^- + p$

(b) $K^- + n \rightarrow K^- + n$

as well as the charge-exchange scattering process

(c) $K^- + p \rightarrow K^o + n$

The possible channels for $K^-$-interactions with one bound nucleon are presented in Table I[13], along with the limits between which the possible values of kinetic energy of the products must lie. Conservation of the system's total momentum is assumed, secondary interactions are neglected, and the internal momentum distribution is assumed Gaussian, with maximum momentum 250 MeV/c. The nucleon binding energy is taken to be 8 MeV.

Eisenberg et. al.[17] used charge dependence to obtain the various complex amplitudes necessary to describe the one-nucleon interaction rates.

Hydrogen bubble chamber work[18] provided the experimental data from which numerical values of the complex amplitudes for $K^-$-proton interactions were obtained. These are presented in the final column of Table I. Those values given for the $K^-$-neutron reactions, 4, 5, and 7 are of course values which have been calculated on the basis of charge independence using the $K^-$-proton experimental data, and neglecting any

Table I. Interaction processes of $K^-$-mesons (at rest) with a single nucleon.

| Process | Q Value MeV | Kinetic energy of products for interaction on a stationary nucleus | | Kinetic energy range for interaction on a nucleon in a nucleus | | Transition Amplitude (Derived in Reference 17) | Branching Ratios |
|---|---|---|---|---|---|---|---|
| | | $T_Y$ (MeV) | $T_\pi$ (MeV) | $T_Y$ (MeV) | $T_\pi$ (MeV) | | |
| 1. $K^-+p \rightarrow \Sigma^+ + \pi^-$ | 103 | 14 | 89 | 0-65 | 30-95 | $\frac{M_0}{6} - \frac{M_1}{2}$ | 0.20 ± 0.01 |
| 2. $K^-+p \rightarrow \Sigma^- + \pi^+$ | 96 | 13 | 83 | 0-50 | 38-88 | $\frac{M_0}{6} + \frac{M_1}{2}$ | 0.44 ± 0.01 |
| 3. $K^-+p \rightarrow \Sigma^0 + \pi^0$ | 106 | 14 | 92 | 0-58 | 40-98 | $\frac{M_0}{6}$ | 0.28 ± 0.03 |
| 4. $K^-+n \rightarrow \Sigma^- + \pi^0$ | 102 | 14 | 88 | 0-51 | 43-94 | $\frac{M_1}{2}$ | 0.08 ± 0.045 |
| 5. $K^-+n \rightarrow \Sigma^0 + \pi^-$ | 102 | 14 | 88 | 0-57 | 37-94 | $\frac{M_1}{2}$ | 0.08 ± 0.045 |
| 6. $K^-+p \rightarrow \Lambda^0 + \pi^0$ | 182 | 29 | 153 | 1-87 | 87-173 | $\frac{N_1}{2}$ | 0.08 ± 0.02 |
| 7. $K^-+n \rightarrow \Lambda^0 + \pi^-$ | 178 | 29 | 149 | 1-87 | 83-169 | $N_1$ | 0.16 ± 0.04 |
| 8. $K^-+p \rightarrow \Lambda^0 + \pi^0 + \pi^0$ | 47 | -- | -- | -- | -- | | |
| 9. $K^-+p \rightarrow \Lambda^0 + \pi^+ + \pi^-$ | 38 | -- | -- | -- | -- | | |
| 10. $K^-+n \rightarrow \Lambda^0 + \pi^0 + \pi^-$ | 43 | -- | -- | -- | -- | | |

effect due to the neutron-proton mass difference.

Dalitz and Tuan[16,19] have treated the low-energy, $K^-$-nucleon interactions by S-wave zero-effective range theory. They obtained four sets of scattering lengths consistent with the then current data[18] on $K^-$-proton interactions.

The complex scattering lengths are given by $A_T = a_T + ib_T$, where the isospin T equals 0 or 1. The complex phase shift, $\delta_T$, is given by $k \operatorname{ctn} \delta_T = (1/A_T)$, where $k\hbar$ is the relative momentum of the $K^-$-nucleon system. The cross sections for the various processes can written in terms of the scattering lengths. Such results are presented in Appendix I, together with those obtained from a more sophisticated treatment[16] which takes into account Coulomb and mass difference effects.

Humphrey and Ross[20] fitted the observed bubble chamber data[18] on the $K^-$-p scattering at low momentum (0-300 MeV/c) to the S-wave zero effective range theory. They determined two possible sets of scattering lengths (amplitudes) $A_0$, $A_1$, which were consistent with the bubble chamber data. The favored solution, however, turned out not to agree with later higher energy data[21,22] or with results of $K^-$-D interaction experiments[23] to be discussed presently.

Sakitt et. al.[15] have redone the low-energy $K^-$-p experiment of Humphrey and Ross[20] with higher statistics. They find that the new data, when combined with existing data and fitted to the zero-effective range theory of Dalitz and Tuan[16], again yield two possible solutions, presented in Table II. This time, however, the solution preferred on the basis of statistical analysis[15] (number 2 in the Table) agrees with the higher energy data[21,22]. In the Table the set of six

parameters which describe the low-energy $K^-$-n interactions are: the scattering lengths $A_0$ and $A_1$; the ratio of $\Sigma^-/\Sigma^+$ production, $\gamma = \Gamma(K^- + p \rightarrow \Sigma^- + \pi^+)/\Gamma(K^- + p \rightarrow \Sigma^+ + \pi^-)$, a function of the phase angle $\varphi$ between the T = 0 and T = 1 channels; and $\epsilon$, the ratio of the $(\Lambda\pi^0)$ production rate to the total hyperon rate in the T = 1 channel.

The error analysis and computations carried out to calculate a minimum value of $\chi^2$ are dealt with in the reference[15], and only the results are quoted in Table II.

The favored solution suggests an S-wave bound state at 1410 MeV which could be associated with the $Y_o^*$ at 1405 MeV. The role of resonances in $K^-$ nuclear interactions will be treated in a later chapter (V).

Hyperfragment formation (IV) and multinucleon processes (III-C) will be dealt with in separate chapters as indicated.

TABLE II. Complex Scattering-Length Solutions

| | $A_0$ (In Fermis) | | $A_1$ (In Fermis) | | | | | |
|---|---|---|---|---|---|---|---|---|
| Solution | $a_o$ | $b_o$ | $a_1$ | $b_1$ | $\gamma\varphi$ | $\epsilon$ | $\chi^2$ | $p(\chi^2)$ |
| 1 | -0.75 | 1.13 | -0.85 | 0.15 | 2.19 | 0.48 | 88.6 | 8% |
| 2 | -1.63 | 0.51 | -0.19 | 0.44 | 2.11 | 0.31 | 76.0 | 38% |

The study of the $K^-$ interaction with the more complicated structure of the deuteron has been carried out in experiments using deuterium-filled bubble chambers; such work has been performed at this laboratory by a section of the Alvarez Group.[23]

The results of that experiment have been analyzed by Schult and Capps,[24] and are presented in Table III. It is shown that certain of the deuteron branching ratios for

(d) $K^- + d \rightarrow \pi + Y + n$

seems to be independent of hyperon-nucleon final state interactions and are related to the branching ratios for $K^-$ in hydrogen.

(e) $K^- + p \rightarrow \pi + Y$

The branching ratios derived in this way do not agree with experimentally observed ones.[18,20]

This discrepancy has been explained by Schult and Capps[24] on the basis of the Dalitz and Tuan scattering length analysis, two solutions of which (the "minus" ones) could lead to an isospin zero resonance in pion-hyperon scattering about 20 MeV below the $K^- + p$ threshold.[19] This explanation is in agreement with the results of Sakitt et. al.[15] who find evidence for an S-wave bound state at 1410 MeV.

TABLE III

Production amplitudes for the seven π-Y-n charge states in terms of the three independent amplitudes, $T_I$, which refer to pure isospin states of πY or Yn.

| Charge State | πY Isotopic-Spin | Yn Isotopic-Spin | Deuterium Events (%) | Hydrogen Events (%) |
|---|---|---|---|---|
| $\pi^+ \Sigma^- n$ | $T_0 + T_1$ | $T_{3/2}$ | 21.4 ± 1.1 | 44 ± 1 |
| $\pi^- \Sigma^+ n$ | $T_0 - T_1$ | $(1/3T_{3/2}+2/3T_{1/2})$ | 21.5 ± 1.8 | 20 ± 1 |
| $\pi^0 \Sigma^0 n$ | $-T_0$ | $-(2/3T_{3/2}+1/3T_{1/2})$ | 28.5 ± 1.3 | 28 ± 3 |
| $\pi^0 \Lambda^0 n$ | $-T_\Lambda$ | $-T_\Lambda$ | | 8 ± 2 |
| $\pi^0 \Sigma^- p$ | $\sqrt{2}\, T_1$ | $\sqrt{2}(1/3T_{3/2}-1/3T_{1/2})$ | 3.2 ± 0.4 | 8 ± 4.5 |
| $\pi^- \Sigma^0 p$ | $-\sqrt{2}\, T_1$ | $-\sqrt{2}(1/3T_{3/2}-1/3T_{1/2})$ | 3.5 ± 0.5 | 8 ± 4.5 |
| $\pi^- \Lambda^0 p$ | $\sqrt{2}\, T_\Lambda$ | $\sqrt{2}\, T_\Lambda$ | 21.6 ± 1.2 | 16 ± 4 |
| Total Events | | | 1646 | 2049 |

## II. OUTLINE OF EXPERIMENTAL PROCEDURE

### A. Exposure and Scanning

The data used in this work were obtained from measurements performed on the interaction stars of negative K-mesons captured at rest by emulsion nuclei.

Two separate emulsion stacks were used. Details on these stacks and their development are presented in Appendix II, containing references 25-28.

The bevatron was the accelerator which produced the negative K-meson beams used in the two stack exposures. The mesons were passed through copper absorbers chosen so that the total mass density was sufficient to bring the beam to rest about midway inside the stack.

The experimental arrangement for the A-stack is presented in Figure 1.

The higher momentum of the $K^-$-meson beam used in the C-stack exposure required more absorber to stop it inside the stack. The emulsion stack was maintained at a constant low temperature (approximately $0^\circ$ C) in order to reduce fading of the latent image and to hinder the growth of fog in the emulsion. The temperature control necessitated certain engineering changes, but the experimental setup is otherwise similar to that in Figure 1.

The $K^-$ capture stars were located by the so-called area-scan method, in which a definite region of each pellicle is searched for the desired type of event. In this case the region was that in which the $K^-$-meson beam was found to come to rest. The beam had been designed to stop in

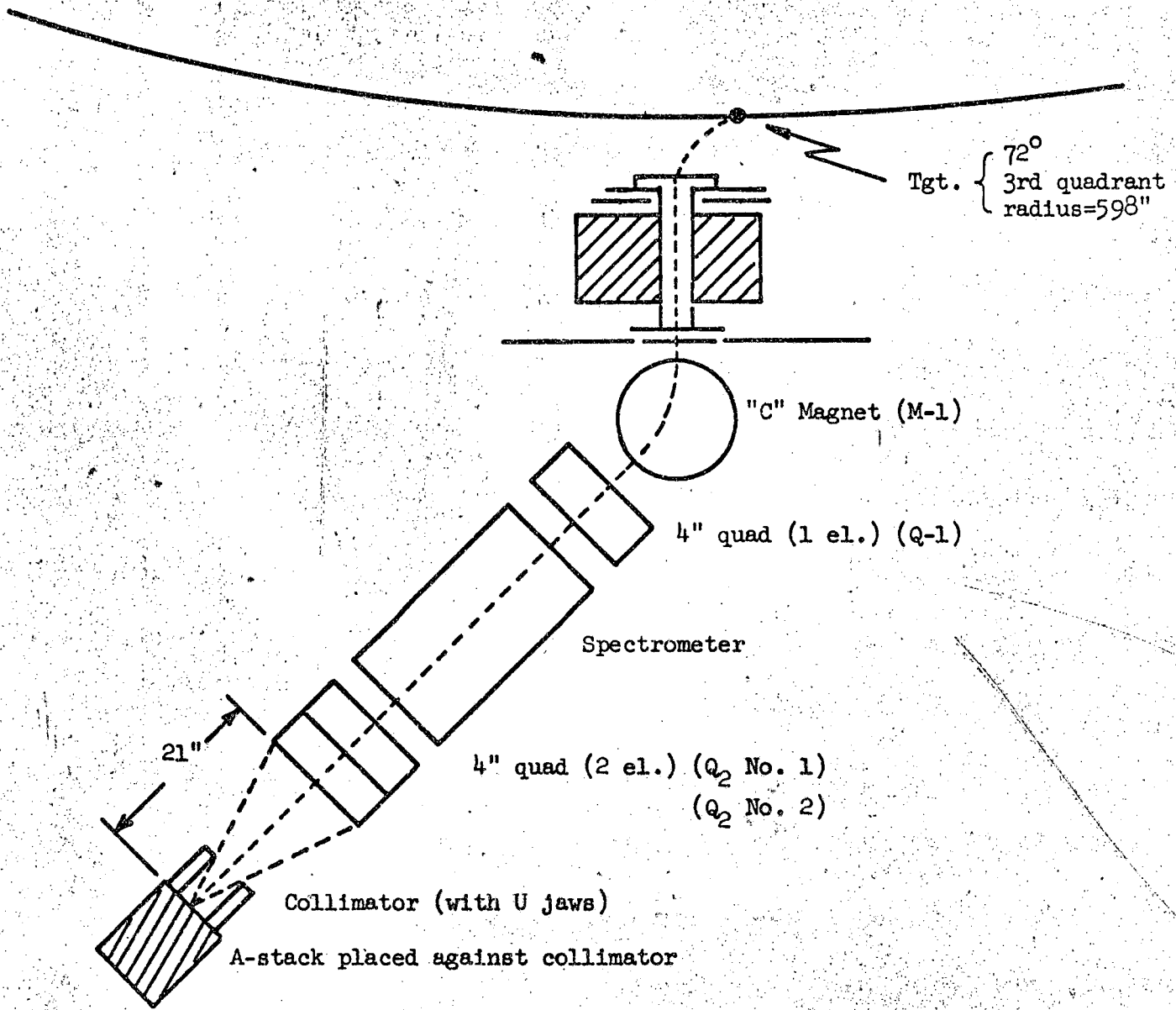


Fig. 1. Experimental Arrangement of the A-stack exposure to the $K^-$-Meson Beam at the Bevatron

a limited region of each stack, thereby considerably reducing the volume of emulsion to be scanned.

The samples of stars found in the two stacks by this kind of scanning of course suffered from a loss of events due to the observational bias against interactions in which no dark prong was produced. The possible errors introduced in the subsequent analysis by this and other kinds of bias will be evaluated in Part B.

The program of analysis in the A-stack will be discussed first, since it was both more extensive and more complete than the subsequent analysis done in the C-stack.

Plates of the A-stack were area-scanned according to a prescribed pattern. Technicians began area-scanning the plates at the center of the incoming beam, as located by prior profile analysis (see Reference 27). Since the beam was fairly narrow in the vertical direction, it was only necessary to scan 20 out of 216 plates in order to accumulate a satisfactory number of events, 2300.

In the A-stack, tracks coming to rest in a given area were recorded provided that they could be identified as K-mesons. This was usually done by following them back for several fields of view and noting the change in ionization. Only for a brief time at the beginning of the A-stack scanning was any attempt made to find zero-prong $K^-$-stars. Thereafter, only those events were recorded which, in addition to satisfying the above criteria, possessed one or more secondary prongs. A prong was defined as a rectilinear collection of grains of length greater than 2.5 microns. Thus there was an incomplete sample (57) of the so-called $K_\rho$ events (zero-prong $K^-$-interaction stars.) These events,

however, were not necessary for the present study.

The story was somewhat different with the scanning of the C-stack. Here all the tracks stopping within a given region and identifiable as $K^-$-mesons were recorded. In this case there were two beam directions since the exposure had been done at two separate times due to technical difficulties with the K-meson beam from the bevatron. During the first exposure the beam had entered the stack from one direction, say $180^\circ$. In the second exposure the beam now entered from $0^\circ$, in order that there be no confusion regarding the age of a particular track. The first exposure was of short duration and the resulting flux of $K^-$ particles was low. Those few interaction stars which were a result of the first exposure were identified readily, and were recorded separately from those produced in the second, longer exposure.

B. Measurements and Data Reduction

1. Recording of data

Data from the A-stack were recorded on McBee Keysort cards, an example of which is shown in Figure 2. Information about the event can be entered both by punching appropriate holes and by writing on the card. The $K^-$-interaction star was located by a scanner and checked by a physicist or experienced technician. The card was then filled out, a sketch of the event made, and appropriate holes punched to describe completely the $K^-$-meson interaction. Further data were then recorded as taken. Results of analysis such as kinetic energy and momentum were also entered on the card. Just as the emulsion itself serves as a permanent record of the $K^-$-meson's interaction, so the Keysort card

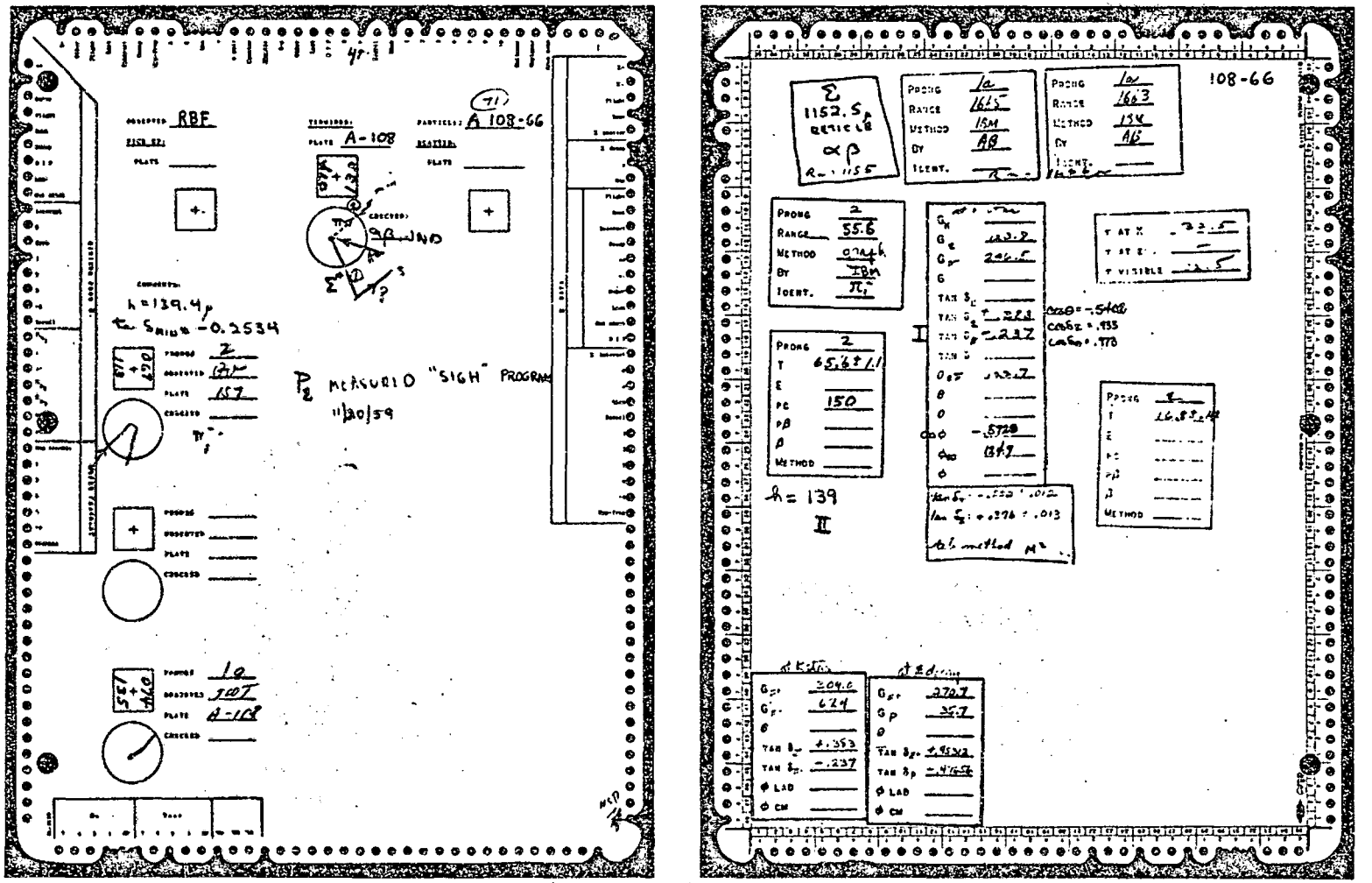


(a) (b)

Figure 2. Reproduction of Keysort Card used to record data. (a) Front Side (b) Back Side

serves as a permanent record of all work done on the event.

For the C-stack the data were handled somewhat differently. All negative K-meson interaction stars, whether at rest or in flight were first recorded on graph paper. This was done by making a pencil dot at the location on the paper corresponding to the grid coordinates of the event. The grid coordinates had previously been photographically printed on the emulsion by methods described in Reference 25. Colored dots were used to designate the various kinds of interaction stars in which the physicists were interested, and only such events were later recorded on the Keysort cards.

Drawings of each event were made on Keysort cards as shown in Figure 2. Other pertinent information was entered as it was obtained: secondary particle identity, momentum, charge, kinetic energy, and dip angle, the height of the $K^-$-interaction above the pellicle mounting-glass, the number of secondary prongs, the presence of an Auger electron, a blob, or a nuclear recoil (a prong shorter than 2.5 $\mu$ ) at the interaction star, and the presence of visibly strange particles among the secondaries. This information was obtained during subsequent analysis.

2. Identification of Events

Events were certified as $K^-$-meson interactions by a physicist or experienced technician. Doubtful events were checked for the incoming track's consistency with beam direction, for its change in ionization with the range and for its multiple scattering at low energies.

Each secondary prong followed out was assigned a tentative identity on the basis of range, ionization, and scattering. In some cases it was not possible to do more than designate the particle as simply a

"baryon".

The methods of identification used for the various kinds of secondary particles differed according to grain density, and employed multiple scattering, differential grain counts, kinematical considerations, and the measurement of track widths. Those tracks which had a grain density higher than that of our criterion were all followed out, and were not difficult to classify as baryon or pion, even when they left the stack, interacted, or decayed in flight. To distinguish $\Sigma$ particles from other baryons was possible for those hyperons which clearly decayed or interacted at rest. Ambiguities in identification of other $\Sigma$ hyperons are discussed further in Chapter III.

The identity of the hyperfragment events was obtained, where possible, by using track-width measurements and by determining the charge both of the hyperfragment decay products and the charge of the $K^-$-interaction nucleus.

All secondary prongs were divided into two classes: In the first group were those having a grain density corresponding to pions of 30 MeV or more kinetic energy, the so-called "minimum" or "light" tracks. In the second group were the remainder of the secondaries, the "gray" and the "black" tracks.

The dip angles were measured for all near-minimum tracks. Only such tracks having dip angles within $\pm 30^{\circ}$ were followed out. Interaction stars emitting minimum tracks which satisfied the above criterion were then subjected to a complete analysis: all secondary particles from these stars were followed out until they came to rest, left the stack, interacted or decayed. The lightly-ionizing particles within

our criteria were followed to rest when possible. Few difficulties were encountered in identifying those which came to rest.

For interactions in flight, tracks which left the stack, and decays in flight, the methods of identification mentioned above: multiple scattering and rate of change of ionization were employed, either singly or in combination with each other. For decays-in-flight it was possible in some cases to follow out the secondary. This procedure identified the primary.

3. Range Measurements

In order to determine the energies of the various particles, accurate measurements of their ranges were required. The energies were then found from a standard range-energy relation.[29]

For short tracks of less than 1 mm, predominantly of baryons, hyperons, and hypernuclei, the ranges were measured by the eyepiece reticle, with dip correction made where necessary. An automatic coordinate read-out microscope,[30] the "range-scope", was used on the longer hyperon tracks, and also for some pions, mainly those associated with $\Sigma$ hyperons. The grid coordinate method described in Appendix III was employed for most of the long-range tracks. The complementary methods of grain density determination and multiple scattering were utilized to obtain estimates of the residual ranges of those particles which interacted, decayed in flight, or left the stack before coming to rest.

Supplementary to the main contribution of this work, a special study was made of the emulsion instrument itself. This work has been published.[31] The A-stack was the object of extensive ionization

calibrations and a grain-density vs velocity curve obtained. This investigation made possible energy determinations of good accuracy. Further details are presented in Appendix IV. The C-stack was later calibrated using these same procedures.

If the length of the track permitted a grain count to be made at two widely separated points (a differential grain count) this was done; otherwise a single determination was made just before the point of interaction.

In some cases the only tool available was multiple scattering. Measurements were performed by the method of optimum constant cells using a digitized Koristka MS2 precision microscope[32] for the most part, although a Cooke multiple scattering microscope[33] was occasionally substituted.

The two methods, grain counting and multiple scattering, were employed in a supplementary fashion where possible, so that two independent estimates of the particle's velocity could be made.

Lightly-ionizing particles are of course more difficult both to locate at the star, and to follow out to rest. This causes a loss of high-energy pions. Its effect on subsequent analysis will be discussed in the next section.

4. Bias considerations

Steps were taken to locate and control systematic error and, where possible, to eliminate it. Since the $K^-$-interaction stars were located by area-scanning rather than edge-scanning, a bias was introduced, for instance, against those events whose only secondary was a lightly-ionizing one.

Fortunately, there was available for comparison a similar stack of K.5 emulsion which had been exposed to roughly the same number of $K^-$-mesons. This stack (designated 2B) had been edge-scanned and the beam tracks followed in until they came to rest, interacted or decayed.

The number of n-prong events, expressed as a percentage of the total number of events in the stack, is presented in Table IV for the seven possible values of n: 0, 1, 2, 3, 4, 5, 6, and $> 6$.

To facilitate comparison of the data with the results from the A-stack, it was necessary to eliminate from the total the number of zero-prong $K^-$-stars. This was so because such events had not been consistently recorded in the scanning of the A-stack. These adjusted percentages, when compared with the corresponding figures for the A-stack, provide an estimate of the degree of bias introduced by area scanning for the various kinds of events. The pertinent numbers are presented in Table IV. The conclusion is drawn that there was an observational loss of one-prong $K^-$-stars in the A-stack. This estimate of the loss then allowed corrections to be made on the data. It was also possible to use the results from the 2B data to obtain an estimate of the total number of zero-prong events in the A-stack, although only a few such events had been recorded in the original data. The results of the foregoing operations are summarized in Table IV.

To facilitate the accurate following out of lightly-ionizing particles, the emulsion plates used in the experiment were positioned, using as guides heavily-ionizing steep tracks which passed through several pellicles. This provided a precise means of matching the

TABLE IV

Prong distribution for emulsion stacks 2B and A. For the A-stack both the observed distribution and the corrected ones are displayed.

| Number of Prongs | 0 | 1 | 2 | 3 | 4 | 5 | 6 | > 6 | Total No. of Events |
|---|---|---|---|---|---|---|---|---|---|
| 2B-Stack (Edge-Scanned) | 348 | 374 | 522 | 384 | 279 | 137 | 79 | 34 | 2157 |
| A-Stack (Area-Scanned) | 57 | 329 | 670 | 529 | 381 | 201 | 110 | 51 | 2328 |
| Number of Prongs as | | | | | | | | | |
| (1) Percentage of total events in 2B-Stack | 16.1 | 17.3 | 24.2 | 17.8 | 12.9 | 6.4 | 3.7 | 1.6 | |
| Percentage error | 0.9 | 0.9 | 1.1 | 0.9 | 0.8 | 0.5 | 0.4 | 0.3 | |
| (2) Percentage of adjusted total (Zero-prong events omitted) for 2B-Stack | -- | 20.6 | 28.9 | 21.2 | 15.4 | 7.6 | 4.4 | 1.9 | |
| Percentage Error | -- | 1.1 | 1.3 | 1.1 | 0.9 | 0.6 | 0.5 | 0.3 | |
| (3) Percentage of adjusted total (Zero-prong events omitted for A-stack. | -- | 14.5 | 29.6 | 23.3 | 16.8 | 8.8 | 4.8 | 2.2 | |
| Percentage Error | -- | 0.8 | 1.1 | 1.0 | 0.9 | 0.6 | 0.5 | 0.3 | |

TABLE IV (Continued)

| Number of Prongs | 0 | 1 | 2 | 3 | 4 | 5 | 6 | > 6 | Total No. of Events |
|---|---|---|---|---|---|---|---|---|---|
| A-Stack (Corrected for lack of zero-prong events and bias against one-prong events) | 455 | 450 | 670 | 529 | 381 | 201 | 110 | 51 | 2847 |
| Percentage of corrected total events in A-stack | 16.0 | 15.8 | 23.5 | 18.6 | 13.4 | 7.0 | 3.9 | 1.8 | |
| Percentage Error | 0.9 | 1.1 | 0.9 | 0.8 | 0.7 | 0.5 | 0.4 | 0.2 | |

pellicle surfaces to each other, and is discussed more fully in References 25 and 28.

Tracks were checked for consistency in grain density and direction when followed from one pellicle to another. A random group of pion tracks was followed back from their termini as a check on the accuracy of our follow-through procedure, and no errors were revealed.

The minimum particles could easily escape detection, especially in a stack having low minimum-grain density such as the A-stack. For this reason, the endings of 100 $K^-$-meson tracks in a random sample were re-examined in order to pick up any associated light tracks which might have been missed in the first observation. The loss of minimums was estimated on this basis to be less than 1 percent.

On this model, as nuclei more complex than hydrogen are encountered by the $K^-$-mesons, the greater absorption of secondary pions in the nucleus and the increasing number of multinucleon interactions cause a decrease in the relative number of charged pions emitted from the interaction stars. Similarly, the charged $\Sigma$-hyperons interact with other nucleons in the process $\Sigma + n \rightarrow \Lambda + n$, so there is a decrease in the relative number of $\Sigma$-hyperons emitted and a corresponding increase in the number of $\Lambda$-hyperons emitted. An absorption rate of about 15 percent for charged pions has been found, while the figure for charged $\Sigma$-hyperons is closer to 50 percent.[10] As the nuclei become more complex, the $K^-$-interactions on neutrons play a more important role and affect the $\pi^-/\pi^+$ and $\Sigma^+/\Sigma^-$ ratios. The existence of the Fermi momentum possessed by the nucleons in the more complex nuclei also causes changes in the ratios, since the branching ratios for the primary

processes in Table I are functions of the phase angle, $\varphi$, between the transition amplitudes T = 0 and T = 1. The phase angle itself is a function of the relative $K^-$-nucleon momentum.[13]

Using events from pion-producing reactions of the kind listed in Table X one may compare in Table XII the various ratios obtained in this work with the values qhoted by the European Collaboration.[10]

As outlined in Chapter II, correction for the observational loss of particles in the extreme zones as a function of energy was made. This consisted of increasing by 29 percent the number of such pion events with energies between 60 and 90 MeV. For pion energies greater than these, the factor was 36 percent.

The adjusted data then yield the ratio of the number of charged pions to the total number of $K^-$-meson events, corrected for observational loss but not for absorption.

An attempt was made to detect any observational loss of stars which was a function of the event's height in the emulsion. The procedure employed was to subdivide on the basis of their height in the emulsion the group of $K^-$ stars possessing 2 or more prongs, that is, the events showing negligible scanning loss according to Table IV. The numbers presented there allowed corrections to be made for the bias against one-prong stars.

The frequency distribution versus height in emulsion for $K^-$-stars having 2 or more prongs is presented in Table V.

TABLE V

Height distribution in emulsion of all $K^-$-stars having 2 or more prongs. All heights were normalized to a pellicle of 600μ thickness.

| Depth in the emulsion (μ above the glass) | 0-100 | 100-200 | 200-300 | 300-400 | 400-500 | 500-600 |
|---|---|---|---|---|---|---|
| Number of stars | 266 | 365 | 343 | 354 | 340 | 274 |

There is some evidence for an observational loss of events near the surface or near the glass. Correction for this bias may be made on the basis of the numbers presented in Table V, if it be assumed with the European Collaboration[10] that there is no loss of particles in the central region of the emulsion. This loss might be expected to increase for tracks of lowest grain density (minimum tracks). It was, therefore, desirable to further investigate the loss of those events yielding minimum tracks, as a function of height in the emulsion. The largest sample of minimum-track events available was that of the pions emitted in the $K^-$-interactions at rest. In Table VI(a) is presented a frequency distribution of the height above the glass mounting of all those events yielding pions of energy greater than 30 MeV.

TABLE VI

Height distribution of $K^-$ stars having associated pions of energy greater than 30 MeV and dip angle less than $30^\circ$. All heights were normalized to a pellicle of 600μ thickness.

| Height in the emulsion (μ above the glass) | 0-100 | 100-200 | 200-300 | 300-400 | 400-500 | 500-600 |
|---|---|---|---|---|---|---|
| a) Number of Pions | 39 | 70 | 64 | 73 | 61 | 42 |
| b) Ratio of zone pions to all stars in zone having 2 or more prongs designated, henceforth, as S2. | 0.147 | 0.192 | 0.187 | 0.206 | 0.180 | 0.153 |
| c) Ratio of zone pions of energy $\leq$ 60 MeV to S2. | 0.075 | 0.082 | 0.078 | 0.084 | 0.079 | 0.076 |
| d) Ratio of zone pions of energy $>$ 60 MeV but $\leq$ 90 MeV to S2. | 0.052 | 0.078 | 0.074 | 0.086 | 0.071 | 0.054 |
| e) Ratio of zone pions of energy $>$ 90 MeV to S2. | 0.020 | 0.032 | 0.035 | 0.036 | 0.030 | 0.023 |

There is again an apparent bias against events near the surface and near the glass. However, the observational loss of events seemed greater for the minimum-track events (Table VI (b)) than for the group of stars having 2 or more prongs (Table V). It was deemed advisable, therefore, to determine whether or not this was indeed the case, and if so, to what extent the loss of minimums exceeded the loss of the dark-prong stars. One method of doing this was to compare the ratios of the

total number of minimum-emitting events (for the most part pions) in a particular height zone to the number of stars in that same zone which have 2 or more prongs. This was done and the ratios are displayed in Table VI(b). The decrease in the number of events in both the top and bottom zones indicates that there is indeed a height-dependent loss of minimum track events which is greater than that for stars having 2 or more prongs. This loss was presumably due to the low grain density of the minimum tracks. To determine the extent to which this was true, the original sample of minimum-emitting events was reduced to one containing only pion secondaries, identified by one or more of the following methods: ionization determination, multiple-scattering, or follow-through. This subsample was further divided on the basis of pion kinetic energy and a comparison was made of the height distribution for pions of energy between 30 MeV and 60 MeV (Table VI(c)), for those of energy greater than 60 MeV but less than 90 MeV (Table VI(d)), and for pions of energy 90 MeV or above (Table VI(e)), The three groups of events included only flat or minimum tracks, that is, those whose dip angle in the emulsion did not exceed $\pm 30^{\circ}$. This angle criterion had been used for the following out of lightly ionizing tracks. A study of the observational loss of events as a function of the dip angle has been done and will be presented separately.

As shown in Table VI(c) for pion energies up to 60 MeV the distribution is fairly flat for the ratios of the number of lightly ionizing pions in a given layer of emulsion to the total number of $K^-$-stars (of 2 or more prongs) in that same height zone. However, the distribution for the ratios taken for the second, more energetic group

of pions (60 MeV to 90 MeV) shows a marked evidence of loss. If the average of the ratios for the four central zones is compared to the average of the ratios for the two extreme zones (surface to bottom), one sees that they differ by around 29 percent, with the loss occurring in the extreme zones. When the third, most energetic group of pions is treated in the same fashion, a slightly higher difference of 36 percent results; therefore, it may be noted that the loss appears to increase with energy, in agreement with the results of the European Collaboration, referred to previously.[10] It is evident that the energy spectra are indeed biased against higher energy pions found in the extreme zones. Accordingly the spectrum shape has been emended by increasing by 29 percent the total number of such pions in the energy interval 60 to 90 MeV, and increasing by 36 percent the number of extreme-zone pions with energy > 90 MeV.

An effort was made to detect any observational loss of events which was a function of the dip angle of the track. The sample of lightly ionizing pions used in the study of bias as a function of height in the emulsion was again utilized. This time, however, all dip angles were included. Although generally only the flat minimum tracks had been followed out, that is, those with dip angle $\leq 30^{\circ}$, dip angles were measured and the grain density was determined for all minimum tracks. The frequency distribution of the dip angle $\delta$ is presented for equal intervals of solid angle in Table VII for all pions of energy greater than 30 MeV or of grain density corresponding to that energy. Up to at least $30^{\circ}$ there seems to be no effect of the dip. There appears to be a 20 percent observational loss of events having dip angles within the

interval $48.6^{\circ}$ to $90^{\circ}$. This is one justification for selecting only flat ones, another being their greater probability of coming to rest in the emulsion stack.

TABLE VII

Distribution of dip angles of lightly-ionizing tracks

| Angle interval (in degrees) | 0-14.5 | 14.5-30 | 30-48.6 | 48.6-90 |
|---|---|---|---|---|
| Number of events | 162 | 168 | 162 | 129 |

# III. EXPERIMENTAL RESULTS

## A. Data

As described in the previous Chapter, all A-stack events were recorded on Keysort cards. Three types of events were selected for analysis:

1. All events exhibiting visible strangeness,
2. All events having pion secondaries, and
3. All events emitting lightly-ionizing proton or pion secondaries corresponding to the grain density produced by a pion of energy 30 MeV or more.

The A-stack data summary is presented below.

TABLE VIII

Characteristics of $K^-$-stars in the A-stack

| Star type | Number of events observed |
|---|---|
| **Visible Strangeness** | |
| $\Sigma^+ + \pi$ | 118 |
| $\Sigma^+ + \text{no } \pi$ | 74 |
| $\Sigma^- + \pi$ | 60 |
| $\Sigma^- + \text{no } \pi$ | 100 |
| $\Sigma^\pm + \pi^+$ | 1 |
| $\Sigma^\pm + \text{no } \pi$ | 59 |
| $HF + \pi$ | 35 |
| $HF + \text{no } \pi$ | 81 |
| **No Visible Strangeness** | |
| $\pi$ | 552 |
| no $\pi$ | 1248 |
| Total Star Types | 2328 |

The data-collecting procedure for the partial analysis of the C-stack was outlined in the previous Chapter. Of the 11 293 $K^-$ interaction stars from that stack which were recorded on graph paper, there were 354 identified $\Sigma$ hyperons which came to rest and were not accompanied by pions. These events were recorded on Keysort cards and, together with the A-stack events, were the subject for analysis of multinucleon $K^-$-captures in emulsion (Part C of this Chapter). The 258 events producing definite hypernuclei were similarly recorded on Keysort cards and provided data to supplement that from the A-stack for the study of the mechanism of hyperfragment production (Chapter IV). There were 824 events of the type consistent with the interaction $K^- + p \rightarrow \Sigma + \pi$ located in our partial survey. After such events were recorded on Keysort cards they were analyzed along with the A-stack data to determine the role of resonance formation in $K^-$-interactions. (Chapter V). It should be noted that less than 10 percent of the stars were classified, i.e. only those within the prescribed criteria were analyzed further. Therefore many, possibly half, of these stars contain strange particles and pions.

The C-stack data are summarized in tabular form as follows:

TABLE IX

Characteristics of $K^-$-stars in the C-stack

| Star Type | | Number of Events Identified in partial survey |
|---|---|---|
| $\Sigma^+ + \pi^-$ | | 86 |
| | $\Sigma^+ \rightarrow \pi^+$ | 36 |
| | $\Sigma^+ \rightarrow p$ | 50 |
| $\Sigma^+ +$ no $\pi$ | | 156 |
| | $\Sigma^+ \rightarrow \pi^+$ | 84 |
| | $\Sigma^+ \rightarrow p$ | 72 |
| $\Sigma^- + \pi^+$ | | 16 |
| $\Sigma^-$ + no $\pi$ | | 198 |
| $\Sigma^\pm + \pi^\pm$ (collinears) | | 129 |
| $\Sigma^\pm$ (flight) | | 91 |
| HF | | 258 |
| Unclassified Stars (This category contains many undetected strange particles and pions) | | 10 359 |
| Total | | 11 293 |

B. Single-Nucleon (1N) $K^-$-Captures

The processes in which a $K^-$-meson interacts at rest with a single nucleon have been listed previously in Table I together with the corresponding branching ratios, but are now repeated in Table X[34] to facilitate comparison with the experimental results obtained from bubble chamber[18,20,23] and nuclear emulsion[10] studies listed here.

The two sets of adjusted results from the $K^-$-Collaboration are presented. In Column I the $\pi$-meson observational loss factor is assumed to be constant and is based on a value of 0.4 for the $\pi^{\pm}/K^-$ ratio. In Column II the constant loss factor is increased by 50 percent for pions with energies above 85 MeV and the $\pi^{\pm}/K^-$ ratio used is 0.44. The first-column values are the ones which are quoted in the literature,[13] however. For the sake of brevity the ratio $\pi^{\pm}/K^-$ will hereafter be called simply the $\pi/K$ ratio.

Errors in the branching ratios are of the order of a few percent.[34] They cannot, therefore, be an explanation for the major differences which exist between the values of the branching ratios for $K^-$-interactions in substances of complexity ranging from hydrogen to emulsion. There are other quantities which differ as well. For example, there is a decrease in the relative number of interactions yielding charged pions and charged $\Sigma$-hyperons. The ratios $\pi^-/\pi^+$ and $\Sigma^+/\Sigma^-$ show marked changes, and there is an increase in the relative number of events yielding $\Lambda$-hyperons.

TABLE X

Branching Ratios for $K^-$-Interactions at Rest

| Interaction | Source of Data: Hydrogen Bubble Chamber[18,20] | Deuterium Bubble Chamber[21] | Nuclear Emulsion: $K^-$ Collaboration[10] I | Nuclear Emulsion: $K^-$ Collaboration[10] II | This work |
|---|---|---|---|---|---|
| $K^- + p \rightarrow \Sigma^+ + \pi^-$ | 20 | 21.6 | 25.6 | 21.5 | 24.4 |
| $K^- + p \rightarrow \Sigma^- + \pi^+$ | 44 | 24.5 | 11.9 | 12.0 | 12.1 |
| $K^- + p \rightarrow \Sigma^o + \pi^o$ | 28 | 20.8 | 14.1 | 12.4 | 14.7 |
| $K^- + p \rightarrow \Lambda^o + \pi^o$ | 8 | 8.0 | 9.4 | 12.1 | 9.5 |
| $K^- + n \rightarrow \Sigma^- + \pi^o$ | -- | 4.6 | 9.1 | 8.9 | 9.0 |
| $K^- + n \rightarrow \Sigma^o + \pi^-$ | -- | 4.6 | 9.1 | 8.9 | 9.0 |
| $K^- + n \rightarrow \Lambda^o + \pi^-$ | -- | 16.0 | 20.8 | 24.2 | 21.3 |

It is of interest here to give the $\Sigma^+/\Sigma^-$ ratio obtained from the number of collinear events in the A-stack. These distinctive-appearing events are due to the interaction of a $K^-$-meson with a free proton in the nuclear emulsion. When correction is made for observational loss of energetic pions, the $\Sigma^+/\Sigma^-$ ratio is found to be 0.40. This compares favorably with the results 0.46 from hydrogen bubble chamber work noted in Table XI.[13] In this Table are presented the values of experimental quantities obtained for $K^-$-interactions in various substances.

TABLE XI

Experimental characteristics of absorption of $K^-$-mesons at rest in various materials

| | | | | Nuclear Emulsion[10] | |
|---|---|---|---|---|---|
| Experimental Quantity | Hydrogen[18] | Deuterium[23] | Helium[35] | $K^-$-Collaboration | This work |
| $\pi^\pm/K$ ratio | 0.64 | 0.67 | 0.55 | 0.40 | 0.38 |
| $\pi^-/\pi^+$ ratio | 0.46 | 1.95 | 5.5 | 3.9 | 3.8 |
| $\Sigma^\pm/K$ ratio | 0.64 | 0.46 | 0.27 | 0.175 | 0.173 |
| $\Sigma^+/\Sigma^-$ ratio | 0.46 | 0.73 | 1.16 | 1.12 | 1.08 |

Explanations for the differences have been advanced by various writers[12,13]. Typically a model is assumed in which most of the primary processes involve interaction with individual nucleons (Table I [13,17]) or with groups of nucleons (See Part C of this Chapter).

On this model, as nuclei more complex than hydrogen are encountered by the $K^-$-mesons, the greater absorption of secondary pions in the nucleus and the increasing number of multinucleon interactions cause

a decrease in the relative number of charged pions emitted from the interaction stars. Similarly, the charged Σ-hyperons interact with other nucleons in the process $\Sigma + n \rightarrow \Lambda + n$, so there is a decrease in the relative number of Σ-hyperons emitted and a corresponding increase in the number of Λ-hyperons emitted. An absorption rate of about 15 percent for charged pions has been found, while the figure for charged Σ-hyperons is closer to 50 percent.[10] As the nuclei become more complex, the $K^-$-interactions on neutrons play a more important role and affect the $\pi^-/\pi^+$ and $\Sigma^+/\Sigma^-$ ratios. The existence of the Fermi momentum possessed by the nucleons in the more complex nuclei also causes changes in the ratios, since the branching ratios for the primary processes in Table I are functions of the phase angle, φ, between the transition amplitudes T = 0 and T = 1. The phase angle itself is a function of the relative $K^-$-nucleon momentum.[13]

Using events from pion-producing reactions of the kind listed in Table X one may compare in Table XII the various ratios obtained in this work with the values quoted by the European Collaboration.[10]

As outlined in Chapter II, correction for the observational loss of particles in the extreme zones as a function of energy was made. This consisted of increasing by 29 percent the number of such pion events with energies between 60 and 90 MeV. For pion energies greater than these, the factor was 36 percent.

The adjusted data then yield the ratio of the number of charged pions to the total number of $K^-$- meson events, corrected for observational loss but not for absorption, which is 922/2847 = 0.32. This is in quite

good agreement with the value of 0.33 obtained by the European Collaboration[10] using a smaller emulsion stack where discrimination between pions and fast protons could not be as certain. Their figure 0.33 was subsequently adjusted to 0.40 from comparison with the results of Amerighi et al.[11] who did a later study in a more favorable stack. The correction was essentially to compensate for the observational loss of energetic pion tracks even in the central zones of the emulsion pellicles, since previous bias considerations had tacitly assumed that there was no loss of particles in these regions. The adjusted data from this work yields a $\pi^{\pm}/K^{-}$ ratio of 0.38, which is in reasonable agreement with their corrected value.

Other quantities of interest may also be formed from the adjusted data. For example, after correction for $\Sigma^{-}$-captures which produced no visible charged prongs,[10] the ratio of the number of charged $\Sigma$-hyperons to the total number of $K^{-}$-mesons, 493/2847 = 0.173, shows close agreement with the European Collaboration result of 0.175 given in Table XI[10,13]. Also, one may calculate the $\Sigma^{+}/\Sigma^{-}$ ratio using the total corrected number of identified $\Sigma$-hyperons from the A emulsion stack. For this ratio we obtain 256/237 = 1.08, in agreement with the corresponding figure 1.12 in Table XI[10,13].

In order to differentiate between $K^{-}$-captures on light nuclei (C,N,O) and those on heavy nuclei (Ag,Br) it was necessary to employ the procedures used with $\pi^{-}$ capture[36,37,38] and with the $K^{-}$-capture[39] by emulsion nuclei. Two criteria are utilized: The difference in height of Coulomb potentials for light (C,N,O) and for heavy (Ag,Br) nuclei and the presence or absence of Auger electrons associated with the capture

stars.

(1) The minimum values of the effective height of the potential barrier for Ag and Br in emulsion are considered to be about 3.3 MeV for protons and about 6.5 MeV for α-particles.[38] In the present emulsion this corresponds to a range of 90 μ for protons and of 30 μ for α-particles. The emission from $K^-$-stars of protons or α-particles with ranges shorter than these values may be interpreted as evidence for capture in a light nucleus of the emulsion. Those stars that have a singly or doubly charged prong of range $< 30$ μ but $> 2.5$μ, the upper limit for the recoil of a nucleus, are thus considered as captures of the $K^-$-meson by a light element. This will give a lower limit to the true number of captures in light elements.

(2) The absence or presence of Auger electrons accompanying the capture of negatively charged particles in nuclear emulsion has been used as one of the criteria for captures in light or in heavy elements of the emulsion respectively. Theoretical[40] and experimental[34,38,41] investigations have shown that the mesic Auger is much commoner in captures on heavy emulsion atoms than in captures on light ones. Indeed, it may be neglected for the light elements, C, N, O.

The results of Condo and Hill[34] have been applied to the present emended data to obtain an estimate of the total number of $K^-$-captures in light nuclei and in heavy nuclei. For the 2847 interaction stars recorded for the A emulsion stack (Table VIII) the percentages obtained by Condo and Hill correspond to 1053 captures on light nuclei and 1794 captures on heavy nuclei.

If it be assumed that the presence of pion secondaries provide

definite identification for $K^-$-interactions with single nucleons, then we may determine the quantity R defined by the ratio

$$R = \frac{\dfrac{\text{Identified } K^- \text{ single-nucleon captures in light nuclei}}{\text{Total number of } K^- \text{ captures in light nuclei}}}{\dfrac{\text{Identified } K^- \text{ single-nucleon captures in heavy nuclei}}{\text{Total number of } K^- \text{ captures in heavy nuclei}}}$$

A ratio of such fractions should eliminate observational loss effects. The numbers determined experimentally are 98 identified interactions on light nuclei and 146 captures on heavy nuclei. There were 10 events in which both a short prong and a possible Auger electron were observed. These events were divided equally between the light nuclei and the heavy nuclei groups.

Forming R then yields

$$R = \frac{\dfrac{98 + 5}{1053}}{\dfrac{146 + 5}{1794}} = \frac{.0978}{.0842} = 1.16$$

in good agreement with the value 1.18 derived from the data of Condo and Hill,[34] using mesonic events as indicators of single-nucleon interactions. Of course R is computed using lower limits for captures on light and on heavy nuclei since a number of pion emission stars are unaccompanied either by short prongs or by Auger electrons. The quantity R does not represent the relative $K^-$-single-nucleon capture probabilities in light and heavy nuclei, but rather it is the ratio of the probability of producing a pion per capture in the light and heavy nuclei.[34] Therefore the number 1.16 means that a $K^-$-capture by a light nucleus is 1.16 times as likely to produce a pion as a $K^-$-capture by a heavy nucleus. This is in agreement with the results of Grote et. al.[39] who found

that the charged-pion emission frequency for $K^-$-captures at rest was of the same order of magnitude for both light and heavy nuclei.

A more satisfying analysis may be made in the case of $K^-$-multi-nucleon captures (Part C) and for the single-nucleon interactions giving rise to pion-emitting stars. This latter case is discussed next. The single-nucleon reactions listed in Table I and again in Table X include two cases where uncharged hyperons are emitted accompanied by negative pions. These reactions are

$$K^- + n \rightarrow \Sigma^o + \pi^-$$

and

$$K^- + n \rightarrow \Lambda + \pi^-$$

and will be treated separately.

A study of the pion kinetic energy spectra of all events (Figure 3 ), was made. The spectra were corrected for energy-dependent observational loss as outlined previously. The number of such pions with kinetic energies between 60 and 90 MeV was increased by 29 percent, while the number with energies greater than 90 MeV was increased by 36 percent. There was a geometrical correction applied to pions with energies greater than 30 MeV. This was necessary since such events had been recorded only if the dip angle was $< 30^o$. The pion dip angle distribution was assumed to be isotropic. In order to normalize the $T > 30$ MeV pion spectra to those events less energetic than 30 MeV (that is, normalize the "flat" ones, recorded only if their dip angle was less than $30^o$), it was necessary to double the number of $T > 30$ MeV events. This was so because half the particles in an isotropic flux would have dip angles between $0^o$ and $30^o$, while the other half would possess dip angles

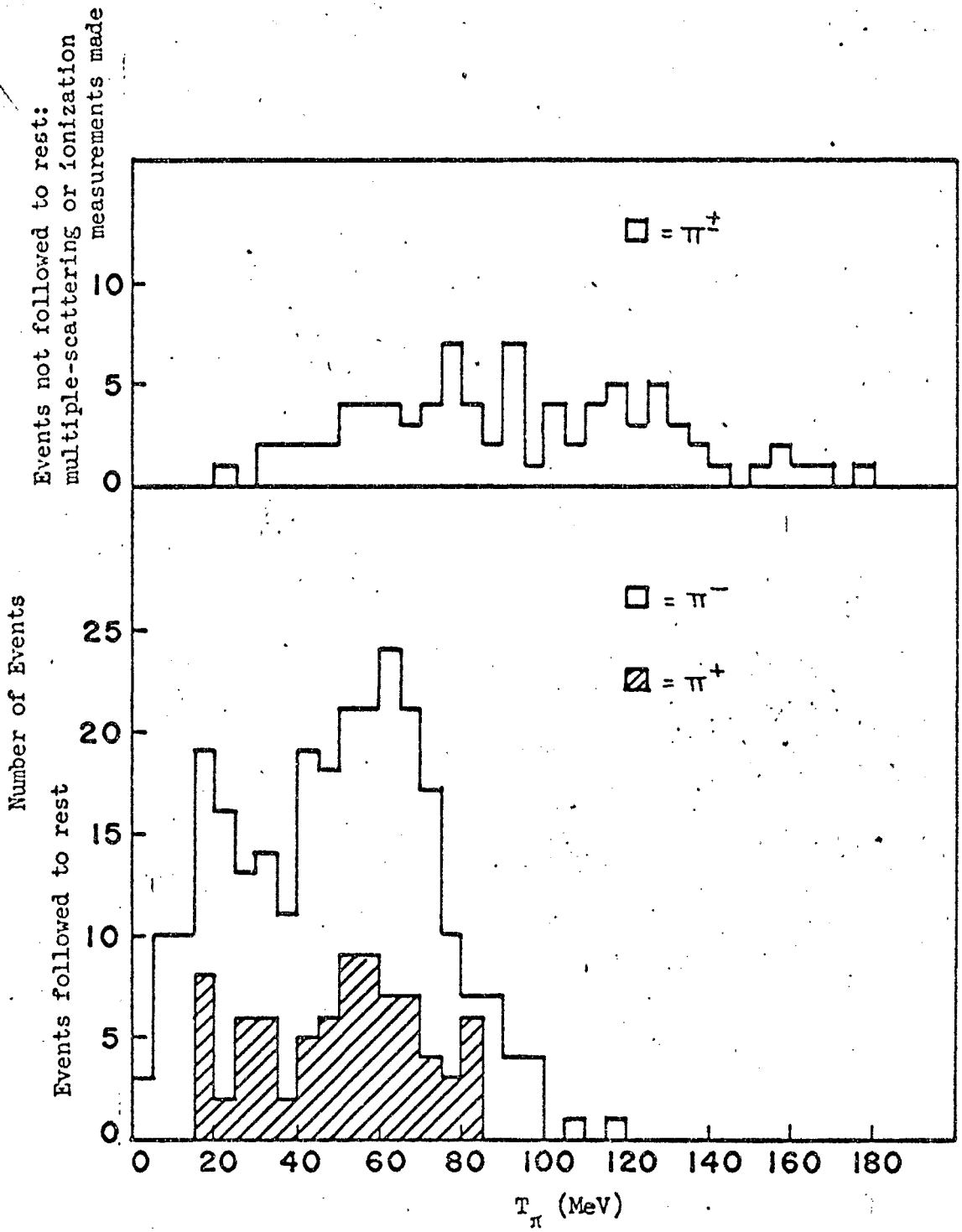


Figure 3. Kinetic energy spectra for all pions within criteria in A-stack

between $30^{\circ}$ and $90^{\circ}$. Before the overall experimental $\pi^-/\pi^+$ ratio is calculated, it is reasonable to form the ratio in several narrower energy intervals, since within a suitable interval there should be negligible bias for either charge. The kinetic energy intervals are 0 to 30 MeV, 30 to 60 MeV, 60 to 90 MeV, and > 90 MeV. One of the advantages of the larger emulsion stack now becomes apparent: a high percentage of secondary pions would come to rest within it. In addition, since lightly ionizing pion tracks were followed only if they were flat (dip < $30^{\circ}$), the percentage of pions stopping within the emulsion was very high: 98 percent for the energy interval 0 to 30 MeV; 90 percent between 30 and 60 MeV; 83 percent between 60 and 90 MeV. For 90 MeV or greater, the percentage fell to 20.

The ratio $\pi^-/\pi^+$ may be formed without correcting the spectra for energy, observational, or geometrical bias, since there should be negligible bias in favor of either sign. In Table XII is presented the uncorrected pion ratios of charged pions, followed to rest and identified as to charge sign, for the various energy intervals. Those pions which did not come to rest were not included here.

TABLE XII

Observed $\pi^-/\pi^+$ ratios for various energy intervals

| Energy of $\pi$ | No. $\pi^-$ | No. $\pi^+$ | Sign Ratio $\pi^-/\pi^+$ | |
|---|---|---|---|---|
| | | | This work | European Collaboration[10] |
| 0-30 | 78 | 16 | 4.9 ± 0.9 | 3.8 ± 0.8 |
| 30-60 | 111 | 33 | 3.4 ± 0.6 | 4.0 ± 0.9 |
| 60-90 | 89 | 27 | 3.3 ± 0.7 | 4.0 ± 1.6 |
| 90-95 | 4 | 0 | --- | --- |
| > 95 | 7 | 0 | --- | --- |

The results of the charge comparisons for the various energy intervals show some disagreement with those of the European Collaboration.[10]

There were two $\pi$-mesons found whose energies, 93 and 94 MeV, were determined from a combination of multiple-scattering and range measurements, since the pion in the former case made a star in flight, and in the latter case disappeared in flight. They were identified as positive solely on the basis of the charge of the accompanying $\Sigma^-$. However, for the first event, the $\Sigma$ itself was a zero-prong event, and was called a negative sigma on the basis of an associated electron at its ending. For the second event, the presence of a short hook ($< 2\ \mu$) at the end of the accompanying baryon served as the basis of identification for the $\Sigma$-hyperon. There were, therefore, no identified positive pions with energies greater than 90 MeV. This result was confirmed in the work done on the study of the hyperfragment production mechanism (Chapter IV). Apart from charge exchange, which may be neglected[10], the only source of positive $\pi$-mesons is the reaction $K^- + p \rightarrow \Sigma^- + \pi^+$. The Q value of

this reaction is 95 MeV, so one would not expect to see positive pions above about 85 MeV from a star emitting a Σ-hyperon. This is borne out by the foregoing experimental data.

In order to calculate the overall experimental $\pi^-/\pi^+$ ratio it was necessary to use the corrected spectra, since the adjustment factors, while constant, are different for the various energy intervals. The corrected total number of identified $\pi^-$-mesons with energy < 90 MeV is 543 events and the like figure for the $\pi^+$-mesons is 150. The overall $\pi^-/\pi^+$ ratio is 3.6 ± 0.3 compared to the figure of 3.9 ± 0.7 obtained by the European Collaboration.[10] However, if, as the present data indicate, the variation in pion charge ratio with energy interval is correct, then the overall ratio is not a meaningful quantity for comparison since the European Collaboration found that the $\pi^-/\pi^+$ ratio remained constant over the entire energy interval 0 to 90 MeV. However, they were not able to follow to rest any pions with energies above 90 MeV, as was possible in this work.

Using the corrected data of the present work allows the calculation of the overall $\pi^-/\pi^+$ ratio for all energy intervals (including > 90 MeV). This figure is 595/158 = 3.8 ± 0.3. If the ratios previously compiled for each energy interval are now used as a basis for apportioning the remaining group of pions of indeterminate charge sign within each interval, one then obtains for the overall $\pi^-/\pi^+$ ratio for all energy intervals 744/178 = 4.2 ± 0.4. This number is in fair agreement with the value found by the European Collaboration. The fact that this number is greater than the one obtained using only charged pions of identified sign is nevertheless to be expected if the pions with energy

greater than 90 MeV are preponderantly of negative sign, as indicated by the results of this work, since the group of pions of indeterminate charge sign consists predominantly of high energy ones.

As stated before, the positive pion is produced only in conjunction with a $\Sigma^-$-hyperon. If $\pi^+$-absorption $p(\pi^+)$ is now assumed to be no more than 15 percent, as is indicated by results of the work done by Bernardini and Levy[42] on the fast proton spectra from pion-capture stars, the total number of $\Sigma^- + \pi^+$ events may be determined from the number of positive pions corrected for geometrical and energy bias, and for absorption, this figure being 204. On the basis of the adjusted number of $\pi^+$-mesons emitted without an accompanying $\Sigma^-$, one can then estimate the absorption probability of the $\Sigma^-$-hyperons as

$$p(\Sigma^-) = \frac{\pi^+ + \text{no } \Sigma^-}{\text{all } \pi^+} = \frac{125}{204} = 0.61$$

Correction should be made for the $\Sigma^-$-hyperons which cannot be identified.[13] This yields a reduction of

$$p(\Sigma^-) \text{ to } \frac{125 - 22}{204} = \frac{103}{204} = 0.50$$

This is in fair agreement with the European Collaboration[10] result $p(\Sigma^-) \approx .45$. From work done on the fast proton spectra of pion-emitting $K^-$-stars, they determine the result $p(\Sigma^-) \approx p(\Sigma^o) \approx p(\Sigma^+)$.

If such a relation is valid then an estimate of the number of $\Sigma^+ + \pi^-$ events may now be made. The number of such events corrected for observational loss was 122. In addition, in the adjusted data there were 60 $\Sigma^+$ events with kinetic energy below 35 MeV. Although

these hyperons were not accompanied by pions, they were nevertheless held to come from single-nucleon reaction channels, since the calculated energy spectrum[10] for $\Sigma^+$-hyperons produced in multinucleon channels indicates a negligible contribution for that energy range. When allowance is made for $\pi^-$ absorption, $p(\pi^-) = 0.15$, and for $\Sigma^+$ absorption, assuming $p(\Sigma^+) \approx p(\Sigma^-) = 0.50$, then an increase to 411 events is obtained for the reaction $K^- + p \rightarrow \Sigma^+ + \pi^-$.

An estimate of the number of $K^- + n \rightarrow \Sigma^0 + \pi^-$ events may be obtained next, following the procedure used by the European Collaboration.[10] The number of one-prong $K^-$-stars yielding $\pi^-$-mesons of less than 50 MeV, designated $(\pi^-,0)$-events, was compared with the number of $\pi^-$-mesons emitted in the same energy range and accompanied only by a $\Sigma^+$-hyperon, the $(\pi^-,\Sigma^+,0)$-events. The adjusted data gave 13.6 for the former number, and 23.2 for the latter. For pions in this energy range (<50 MeV), any contribution from the reaction $K^- + n \rightarrow \Lambda + \pi^-$ may be neglected.[10] The only correction applied is then one for zero-prong events arising from the interaction $\Sigma^0 + n \rightarrow n + \Lambda$, and is made by analogy with the derivation of the $\Sigma^-$-absorption probability. That is, there were 30 $\pi^+$-mesons identified in the chosen energy interval, and only 7 had no associated prongs. If it be assumed that half of the emitted $\Sigma^0$-hyperons interact with neutrons, and that $p(\Sigma^0) \approx p(\Sigma^-)$, then we expect $3.5/23 = 0.14$ of the $\Sigma^0$ to be absorbed in such a manner as to produce a zero-prong star. Little difference is expected between the $\pi$-meson energy spectra of $\pi^- + \Sigma^+$ and $\pi^- + \Sigma^0$ events, or between the associated stable prong distributions. This allows one to form the ratio

$$\frac{\pi^-,\Sigma^o}{\pi^-,\Sigma^+} = \frac{13.6 \times (1-3.5/23)}{23.2 + 8} .$$

For the numerator, the data must be corrected by the probability $1.0-\frac{3.5}{23}$ that a $\Sigma^o$-absorption produces a zero-prong event, while in the denominator the observational loss of $\Sigma^+$-hyperons for this sample of events must be compensated for. The result is

$$\frac{\pi^-,\Sigma^o}{\pi^-,\Sigma^+} = \frac{11.6}{31.2} = 0.37$$

in fair agreement with the value 0.34 obtained by the European Collaboration.[10] From the number of $\Sigma^+ + \pi^-$ events already obtained, one may then calculate that the reaction channel $K^- + n \rightarrow \Sigma^- + \pi^o$ contributes 152 events. The total number of $\pi^-$-mesons contributed by the two channels $K^- + p \rightarrow \Sigma^+ + \pi^-$ and $K^- + n \rightarrow \Sigma^o + \pi^-$ is then 411 + 152 = 563. However the total number of negative pions from all channels, corrected for absorption is 922. One may estimate, therefore, the number of events contributed by the remaining $\pi^-$-producing reaction channel $K^- + n \rightarrow \Lambda + \pi^-$. The result is 359.

Calculations based on charge independence[10] then allowed the numbers for the remaining channels to be determined.

For the reaction $K^- + p \rightarrow \Lambda + \pi^o$ the number 159 was deduced, and correspondingly, for the other two channels $K^- + p \rightarrow \Sigma^o + \pi^o$ and $K^- + n \rightarrow \Sigma^- + \pi^o$, we have 248 and 152 respectively.

These results are tabulated and presented in Table XIII, along with those from the European Collaboration[10] for purposes of comparison.

TABLE XIII

Results for $K^-$-meson interactions at rest in nuclear emulsion: The single-nucleon channels

| Reaction | Corrected No. of events | Branching ratios This work | European Collaboration[10] I | II |
|---|---|---|---|---|
| $K^- + p \rightarrow \Sigma^+ + \pi^-$ | 411 | 24.4 ± 2.5 | 25.6 ± 3.0 | 21.5 ± 2.6 |
| $K^- + p \rightarrow \Sigma^- + \pi^+$ | 204 | 12.1 ± 2.3 | 11.9 ± 2.8 | 12.0 ± 2.7 |
| $K^- + p \rightarrow \Sigma^o + \pi^o$ | 248 | 14.7 ± 3.6 | 14.1 ± 5.1 | 12.4 ± 4.5 |
| $K^- + n \rightarrow \Sigma^- + \pi^o$ | 152 | 9.0 ± 2.1 | 9.1 ± 3.0 | 8.9 ± 2.9 |
| $K^- + n \rightarrow \Sigma^o + \pi^-$ | 152 | 9.0 ± 2.1 | 9.1 ± 3.0 | 8.9 ± 2.9 |
| $K^- + p \rightarrow \Lambda + \pi^o$ | 160 | 9.5 ± 1.2 | 9.4 ± 1.3 | 12.1 ± 1.8 |
| $K^- + n \rightarrow \Lambda + \pi^-$ | 359 | 21.3 ± 2.9 | 20.8 ± 3.2 | 24.2 ± 3.5 |

C. Multinucleon (2N) $K^-$ Captures

In Table XIV[13] are presented the non-mesic or multinucleon $K^-$-interaction processes.

TABLE XIV

Interaction Processes of $K^-$-Mesons with Two Nucleons

| Process | Q value MeV | Kinetic energy of products for interaction on stationary nucleons $T_Y$ (MeV) | $T_N$ (MeV) | Transition amplitude |
|---|---|---|---|---|
| 1) $K^- + p + p \rightarrow \Sigma^+ + n$ | 241 | 107 | 134 | $1/3(M_{3/2} + 2M^{(1)}_{1/2})$ |
| 2) $K^- + p + p \rightarrow \Sigma^o + p$ | 241 | 106 | 135 | $(2^{1/2}/3)(M_{3/2} - M^{(1)}_{1/2})$ |
| 3) $K^- + p + n \rightarrow \Sigma^- + p$ | 237 | 105 | 132 | $(2^{1/2}/3)(M_{3/2} - M^{(1)}_{1/2}) - -(2/3)^{1/2} M^{(0)}_{1/2}$ |
| 4) $K^- + p + n \rightarrow \Sigma^o + n$ | 241 | 106 | 135 | $(1/3)(2M_{3/2} + M^{(1)}_{1/2}) + + (1/3)^{1/2} M^{(0)}_{1/2}$ |
| 5) $K^- + n + n \rightarrow \Sigma^- + n$ | 237 | 105 | 132 | $M_{3/2}$ |
| 6) $K^- + p + n \rightarrow \Lambda^o + p$ | 317 | 147 | 170 | $(2/3)^{1/2} N^{(1)}_{1/2}$ |
| 7) $K^- + p + n \rightarrow \Lambda^o + n$ | 317 | 147 | 170 | $N^{(0)}_{1/2} - (1/3)^{1/2} N^{(1)}_{1/2}$ |

The kinetic energy spectra of Σ-hyperons from such interactions extend well beyond those of the Σ-hyperons from the one-nucleon interaction processes. The only sure indication that one is in fact dealing with a multinucleon interaction is the presence of a Σ-hyperon whose kinetic energy is greater than 60 MeV.[34] In the present work, the kinetic energy spectra of all Σ-hyperons unaccompanied by pions, presented in Figure 4, were studied and limits placed on the proportion of such non-mesic processes. In addition the ratio R, defined in the

Figure 4. Kinetic energy spectra of Σ-hyperons in A-stack (a) Accompanied by pion secondary

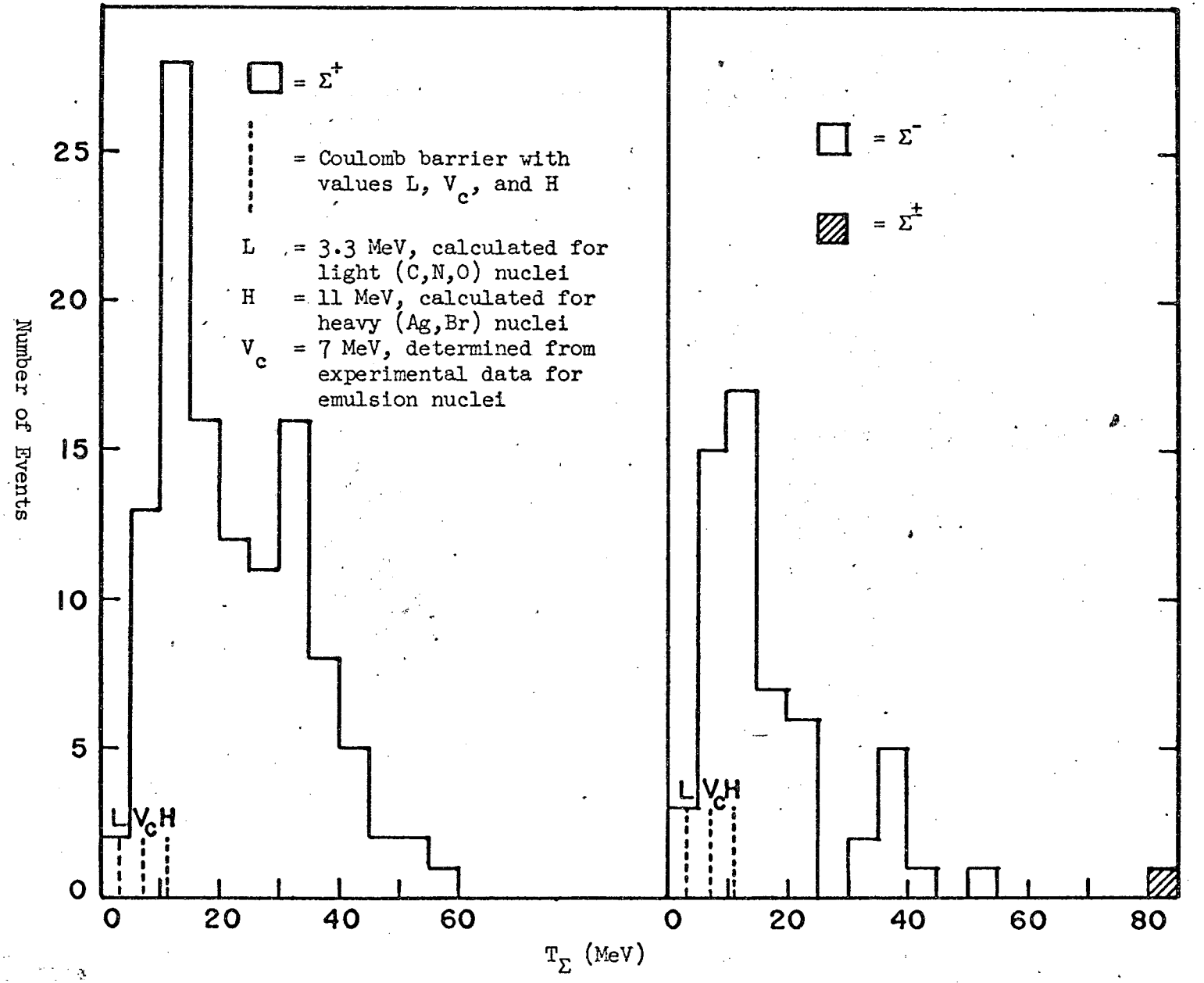

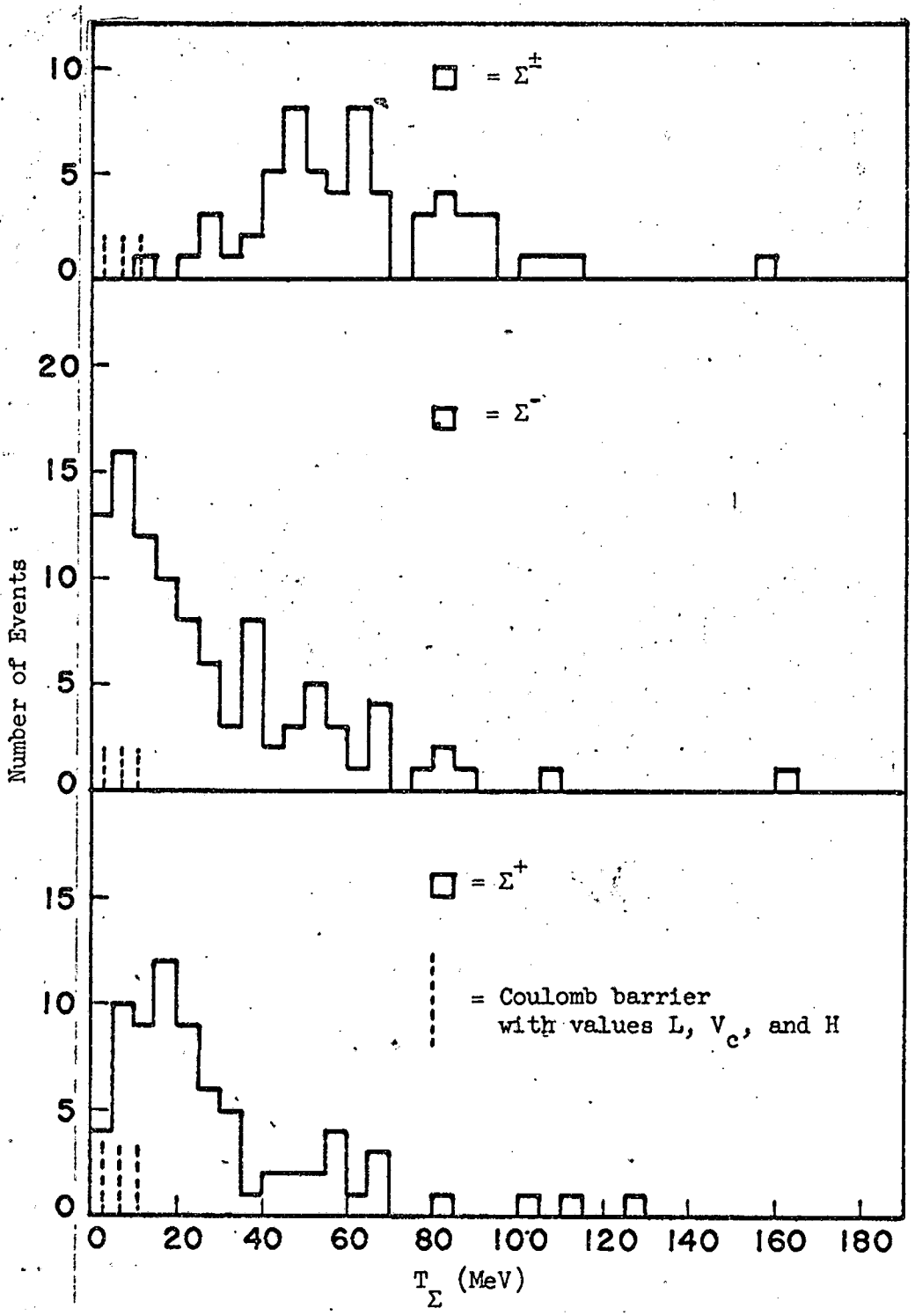


(b) Unaccompanied by pion secondary

previous section, was computed for the multinucleon capture rate.

In leaving the nucleus the Σ-hyperons are displaced in energy by the Coulomb potential; the $\Sigma^+$-hyperons are increased in energy by $V_c$ and the $\Sigma^-$-hyperons are decreased by the same amount. Although the magnitude of $V_c$ varies depending on whether the nucleus is light (3 MeV) or heavy (11 MeV), the effective value consistent with experimental results is 7 MeV.[10] At low energies the hyperon spectra are distorted: a number of $\Sigma^-$-hyperons are trapped in the nucleus, while the $\Sigma^+$-energy distribution is cut off on the low-energy side. Those $\Sigma^+$-hyperons with energy less than 7 MeV probably arise from interactions in light nuclei.[10] The high-energy ends of the $\Sigma^-$ and $\Sigma^+$ kinetic energy distributions should not be distorted by the Coulomb barrier but only displaced in energy. The numbers of hyperons with kinetic energies greater than 60 MeV (fast hyperons), corrected for the Coulomb barrier effect, were as follows: 4 $\Sigma^+$, 21 $\Sigma^-$, and 29 $\Sigma^\pm$. Upper and lower limits were obtained for the true proportion of multinucleon primary capture processes.

From the adjusted data, the upper limit was taken to be the ratio of the number of hyperons unaccompanied by a meson, taking into account pion absorption, to the number of all hyperons observed, 228/493 = 0.46, in fair agreement with the value 0.40 obtained by the European Collaboration.[10] Correction for hyperon absorption was not made, since such a multiplicative constant in both numerator and denominator would cancel. In similar fashion, the lower limit was taken to be the ratio of the number of fast hyperons, corrected for the Coulomb barrier effect, to the total number of hyperons, 54/493 = 0.11, while the like value found by the European group[10] was 0.09.

Differentiation between captures on light and on heavy nuclei was made by means of the criteria established in the previous section, that is, the presence of prongs shorter than 30 μ but longer than 2.5 μ and the presence of Auger electrons.

The quantity R has been computed, omitting the absorption correction, since it would cancel in the ratios.

$$R = \frac{\dfrac{\text{Identified } K^- \text{-multinucleon captures in light nuclei}}{\text{Total number of } K^- \text{-captures in light nuclei}}}{\dfrac{\text{Identified } K^- \text{-multinucleon captures in heavy nuclei}}{\text{Total number of } K^- \text{-captures in heavy nuclei}}}$$

$$= \frac{\frac{2.15}{1053}}{\frac{15.5}{1794}} = 2.36 \pm 0.60$$

This is larger than the result obtained in the work of Condo and Hill[34] which was 2.0 ± 0.5, while it is smaller than that of Evans et. al.,[43] 2.59 ± 0.47. However, a "best" value of R based on their own data combined with that of Evans et. al. has been obtained by Condo and Hill[34] and is given here for comparison, R = 2.22 ± 0.28. This is in agreement with the result of this work.

The results of the forementioned authors, confirmed in the present analysis, show that apparently a $K^-$-capture by a light nucleus is more than 2 times as likely to produce a fast hyperon as is a $K^-$-capture by a heavy nucleus.

# IV. HYPERFRAGMENT PRODUCTION

## 1. Introduction

Lambda hyperons are known to be attracted by nuclear matter to form bound states with all stable nuclei except the nucleon itself. The Λ-nuclei systems are referred to as Λ-hypernuclei or hyperfragments (HF).

During the last decade, considerable work has been done on the analysis of hyperfragments but less has been done on the actual mechanism of hyperfragment formation.[44-52] Although many authors have speculated on different mechanisms of hyperfragment formation, the lack of experimental data precluded the favoring of one model over another.[48, 49,53,54] Until now, also, few direct measurements have been made on the interaction between the nucleon and the Λ-hyperon.

An investigation of the mechanism of hyperfragment formation in $K^-$-capture at rest in emulsion nuclei has been made by the author in collaboration with P. L. Jain of the New York State University at Buffalo, and the results, in part reproduced here, have been published.[55] The hyperfragments are identified with greater certainty by studying the parent star as well as the hyperfragment decay (Sects. 2 and 3). This type of study of parent stars also helps greatly in checking the identity of the produced hyperfragments, which are customarily identified from their decay schemes. By reason of the criteria used in certifying the hyperfragments (a discernible prong emitted from the nucleus), the analysis excluded those hyperfragments which are themselves the residual nuclei; no cryptofragments are included. In Section 4 is discussed the analysis of parent stars produced by $K^-$-capture in emul-

sion nuclei; determination of the relative number of hyperfragments produced in light (C,N,O) and in heavy (Ag,Br) elements of the emulsion is emphasized. Properties of hyperfragments are discussed in Section 5. In Section 6, the primary reactions involving the production of HF are considered.

## 2. Experimental Procedure

As mentioned in Chapter III of this work, the two emulsion stacks A and C had been exposed at separate times to $K^-$-meson beams from the bevatron, and the resulting interaction stars provided the basis for this hyperfragment analysis. All events in which a stopping $K^-$-meson produced a double star of a recognizable hyperfragment were recorded.

Of approximately 13,000 $K^-$-stars there were 63 hyperfragment events, discerned as having been emitted from the parent nucleus and possessing an associated pion, or a fast ($T > 30$ MeV) proton with or without an accompanying pion, the dip angle of the proton or pion being less than $30^\circ$, except for pions of less than 30 MeV, in which case no restriction on dip angle was made. Of the total 63 events selected for analysis, 35 had a pion, 19 had fast protons but no pions, and 9 had both a high-energy proton and an accompanying pion. All the prongs of the parent stars of the 63 events were followed until they interacted, came to rest, or left the stack. The dimensions of the stack were large enough that no proton track left the stack. All but 16 pion tracks were followed to their ends. Of these, only eight interacted or left the stack while still possessing a residual range greater than 1 cm, as determined from ionization or multiple scattering measurements.

3. Energy Determination

The energies of stopping particles were determined most accurately by measuring their ranges. In the few cases for which there was much scattering at the end of the track, a range microscope was used for the measurement of the last portion of the track.[30]

The residual energy of particles that either left the stack or interacted in flight was estimated by ionization measurements made in pellicles that had been the subject of extensive calibrations. Barkas[28] has derived a rather complete statistical theory of track structure in emulsion; this theory was used for determining the ionization of tracks. For heavy ions the range-energy relationship of Heckman et. al.[56] was used. These data, determined for a wide variety of ions, are adjusted for the effects of electron pickup and are very useful for the short tracks with which one is here concerned. Where possible multiple scattering measurements were made to check the ionization determinations.

4. Production of Hyperfragments from Light and Heavy Elements

The procedures previously used, outlined in Chapter III, have been followed in order to distinguish between a $K^-$-capture in light (C,N,O) and in heavy (Ag,Br) elements of the emulsion. These procedures make use of (a) the difference in height of Coulomb potentials for light and for heavy nuclei, and (b) the presence or absence of Auger electrons associated with the capture stars.

(i) Stars which emit a singly or doubly-charged prong of range $< 30\ \mu$ are considered to be $K^-$-meson disintegrations of a light element. The number of such events will of course be only a lower

limit to the true number of captures in light elements. A plot is made in Figure 5 of the range distribution of the shortest track connected with a $K^-$-capture star. The ranges of all prongs are greater than 2.5 $\mu$, which is considered the upper limit for the recoil of a nucleus. The fraction of hyperfragment parent stars that probably originated in C, N, or O is large, and it appears to increase with the charge Z of the hypernucleus emitted; with $Z \geq 5$ the distribution is composed entirely of hyperfragments. Investigations by Abelado et. al.[47] on mesonic HF have shown that the emission spectra of $^8$Li and $_\Lambda$Li are similar. According to their estimation, based on the fraction of $^8$Li having short prongs, at least 75 percent of the mesonic Li originate in the light elements. They further deduce that the contributions to the observed short prong spectra by $Z > 2$ isotopes may be accounted for by assuming for these, on the average, range spectra similar to the one observed for $^8$Li. Production of light HF predominantly on C, N, O is therefore implicitly confirmed. There is a possibility that light hypernuclei $_\Lambda$H or $_\Lambda$He may be produced in $K^-$-capture in heavy nuclei, but HF emitted with $Z > 3$ may be ruled out, since the depth of the nuclear potential normally is too great to be overcome. The fraction of $\Lambda$-hyperons trapped in nuclei may be quite large, since often the hypernucleus may be created with such small kinetic energy that it does not produce a track that can be detected. Such hypernuclei or cryptofragments have been estimated, by one report, to form as much as 30 ± 7 percent of $K^-$-interactions in emulsion nuclei, while another report indicates that the percentage is $13^{+15}_{-13}$; there is, however, general agreement that the fraction of cryptofragments produced is greater than the 5 percent

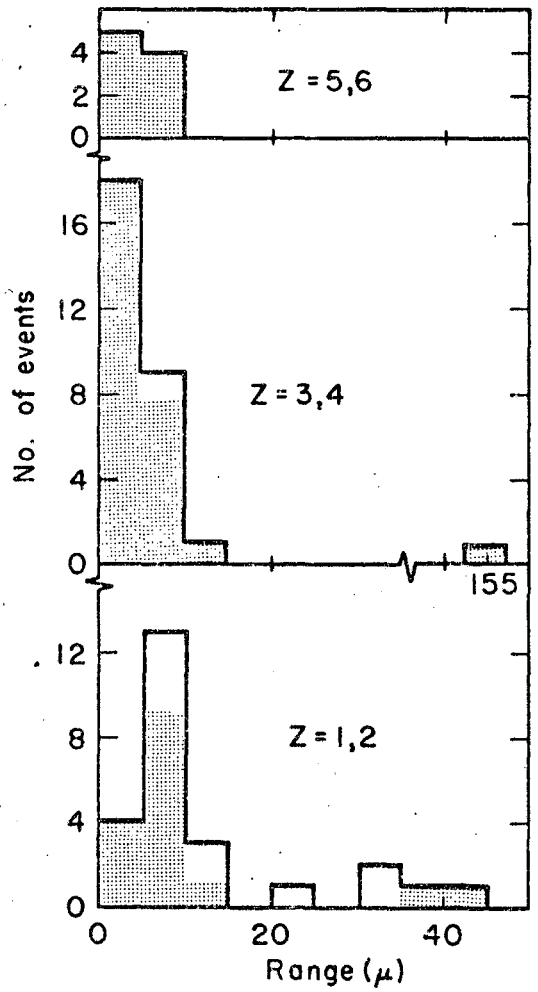


Fig. 5. Range distribution of the shortest prong (> 2μ) from $K^-$-stars at rest, associated with hyperfragments of charge Z. The shaded area indicates events in which the shortest prong is the hyperfragment itself.

figure for identified HF.[10,13]

(ii) The presence of Auger electrons is considered evidence for the $K^-$-disintegration of heavy nuclei.

The center of each of the 63 parent stars was checked in a search for Auger electrons. All blobs having four or more grains were noted, since such a blob may be an electron with energy of about 16 keV produced by the cascading $K^-$-meson. Out of a total of 63 parent stars having hypernuclei only two events were found with definite electrons and two events with probable Auger electrons. The background formed by random electron tracks at the star was considered negligible. Since from this total of four Auger events none were identified as being definitely an example of $K^-$-capture on a light nucleus, the use of the presence of an Auger electron as one indicator of $K^-$-absorption on a heavy nucleus was felt to be justified; this criterion is in agreement with the works quoted above. In as much as there were found only 12 hyperfragments whose range, charge, and concomitant-prong ranges were of the right magnitude to allow them to be classed as possibly coming from heavy nuclei, it is estimated that an upper limit of 19 percent (12/63) may be placed on the fraction of light hyperfragment ($Z < 7$) production taking place in heavy elements (Ag,Br). It should be noted that quite a large number of heavy hypernuclei with charge between $Z = 35$ and $Z = 47$ are formed,[13] but these are not detected by the foregoing analysis. These heavy HF therefore cannot be included in the data by means of which the upper limit is fixed. In Figure 6 is shown the prong-number distribution of parent stars containing hyperfragments of $Z = 1, 2, 3, 4, 5$, or 6.

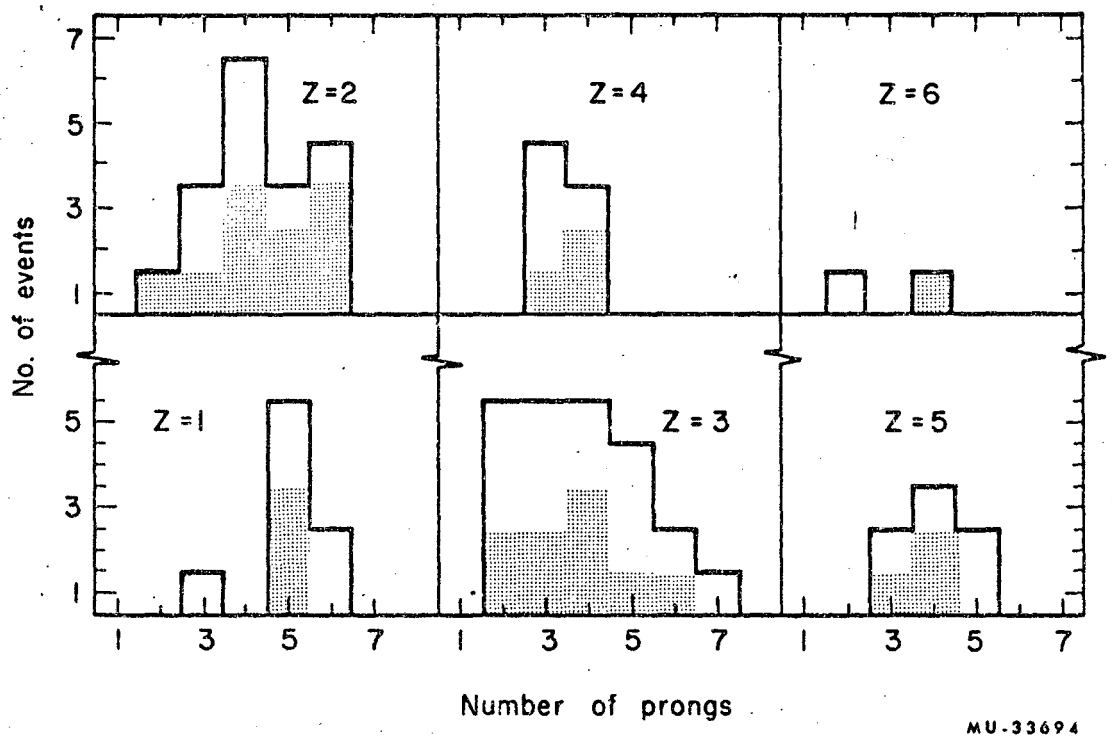


Fig. 6. Prong-number distribution of the parent stars of HF of charge Z = 1, 2, 3, 4, 5, and 6. The shaded areas (mesic HF) indicate that a $\pi^-$ was emitted from the $K^-$-star in association with the HF. Use is made of this information in estimating the total charge of the parent star from the prongs making up the star.

5. Details of Hyperfragments

In Figure 7 (a) is shown the histogram of Z values of the hyperfragments whose production was associated with at least one charged, fast particle ($\pi$ or p). The shaded portion corresponds to mesic HF. Mesic hypernuclei predominate for Z = 1, and for Z > 1 the nonmesic HF are more abundant, in agreement with observations by many others. The charge value Z of each hyperfragment was measured from the total visible charge of its disintegration products, obtained either from ionization determinations or track-width measurements. Width measurements on the tracks of the hyperfragment were also made when possible in order to check the charge estimate. Figure 7 (b) gives the range distribution for all hypernuclei that came to rest. Around 90 percent of the HF have a range less than 45 $\mu$.

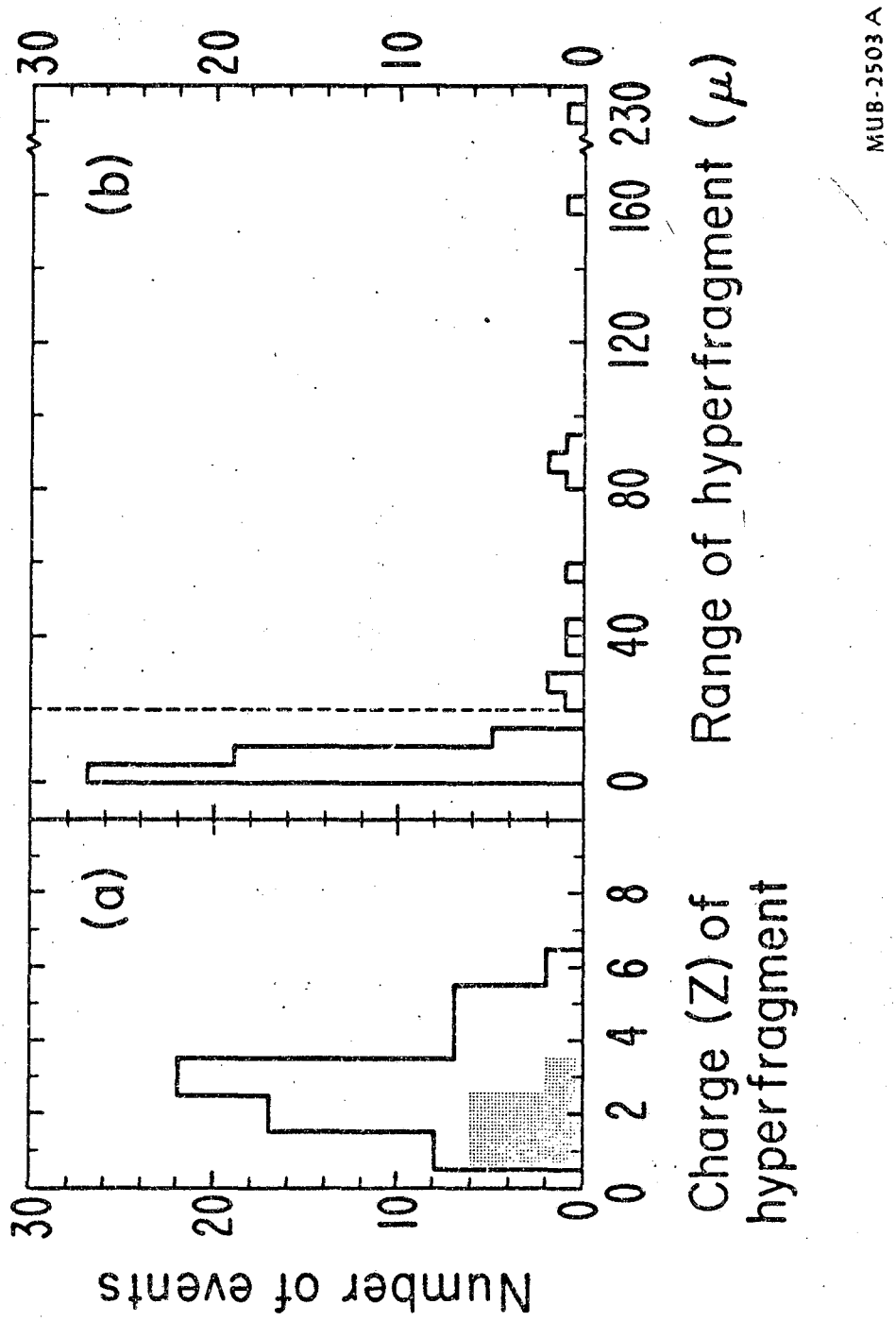


Fig. 7(a) The charge distribution of hyperfragments. The shaded area (mesic HF) gives information on whether the hyperfragment is mesic or nonmesic. (b) Range distribution of the hypernuclei studied in this report. The Coulomb barrier lower limit for emission of a charged particle with $Z > 1$ from a heavy nucleus is indicated by the dashed line.

The momentum spectrum of all hyperfragments is shown in Fig. 8. For comparison the normalized momentum distribution of free Λ's from $K^-$-captures in He is also shown.[35] Lower momentum values are assumed to be mostly from the Σ-conversion events, whereas higher momentum values supposedly come from direct Λ events. Although the average momentum expected from a single-nucleon $K^-$-capture is about 250 MeV/c, it is about 580 MeV/c from a two-nucleon capture, with some spread due to the Fermi motion of the nucleons. There are more low-momentum hyperfragment events. Such a difference between the two spectral shapes may be due to Σ-conversion. The relation between hyperfragment momentum and the cosine of the space angle φ between the hyperfragment and associated pion or proton ($T_p > 30$ MeV, where $T_p$ is the kinetic energy of the proton) is shown in Fig. 9. It indicates that hyperfragments of higher momenta tend to be preferentially emitted at large angles with respect to the pion or fast proton. Since to conserve momentum this is expected, no further interpretation of it is made.

Figure 10 is a plot of average fast proton or pion momentum versus associated HF charge. The two distributions are quite similar. The proton distribution stays close to 400 MeV/c and the pion distribution is fairly constant at 160 MeV/c.

6. Primary Reactions Involved in HF Production

The following general reactions produce Λ-hyperons when $K^-$-mesons are captured by emulsion nuclei. The symbol N represents a nucleon, either a proton or a neutron, while π and Σ stand for the positive or negative charge state of the pion and hyperon, respectively, as necessary to balance charge in the given equation. The reactions

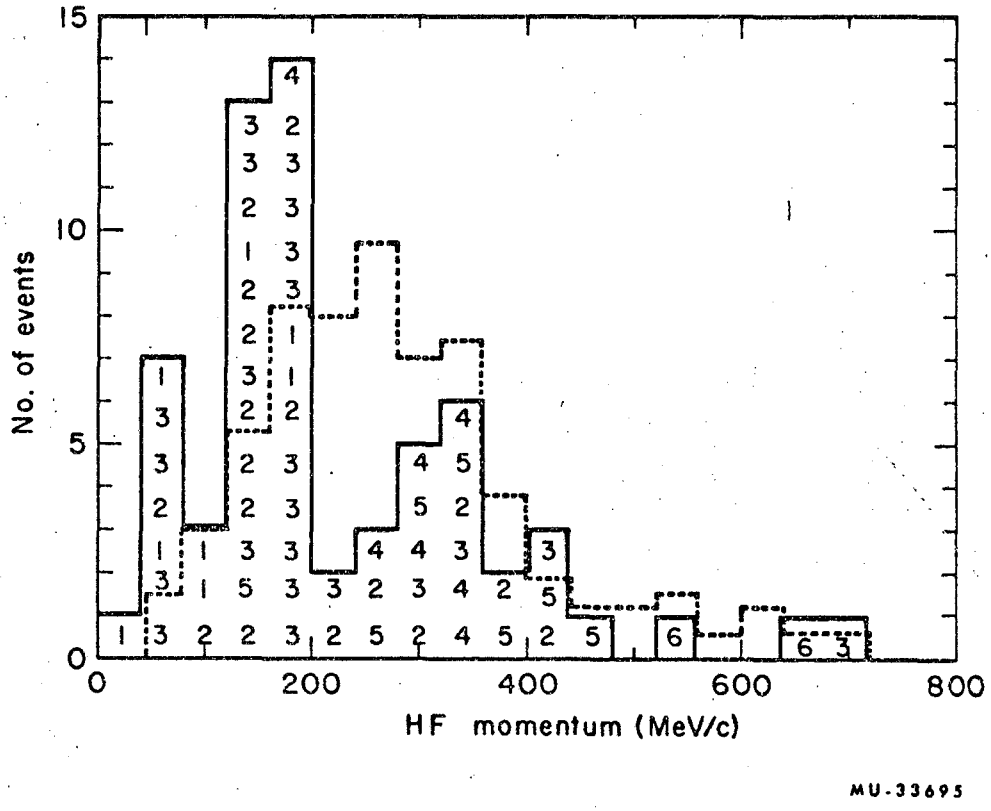


Fig. 8. Momentum spectrum of the emitted hyperfragments (whose charge is indicated by a number in each square of the histogram) from $K^-$-captures at rest in nuclear emulsion, compared with the momentum spectra of free $\Lambda$'s from $K^-$-capture in He (according to Helium Bubble Chamber Collaboration Group). The spectra are normalized to equal areas: full line, HF; dashed line, $\Lambda$ particles in He bubble chamber.

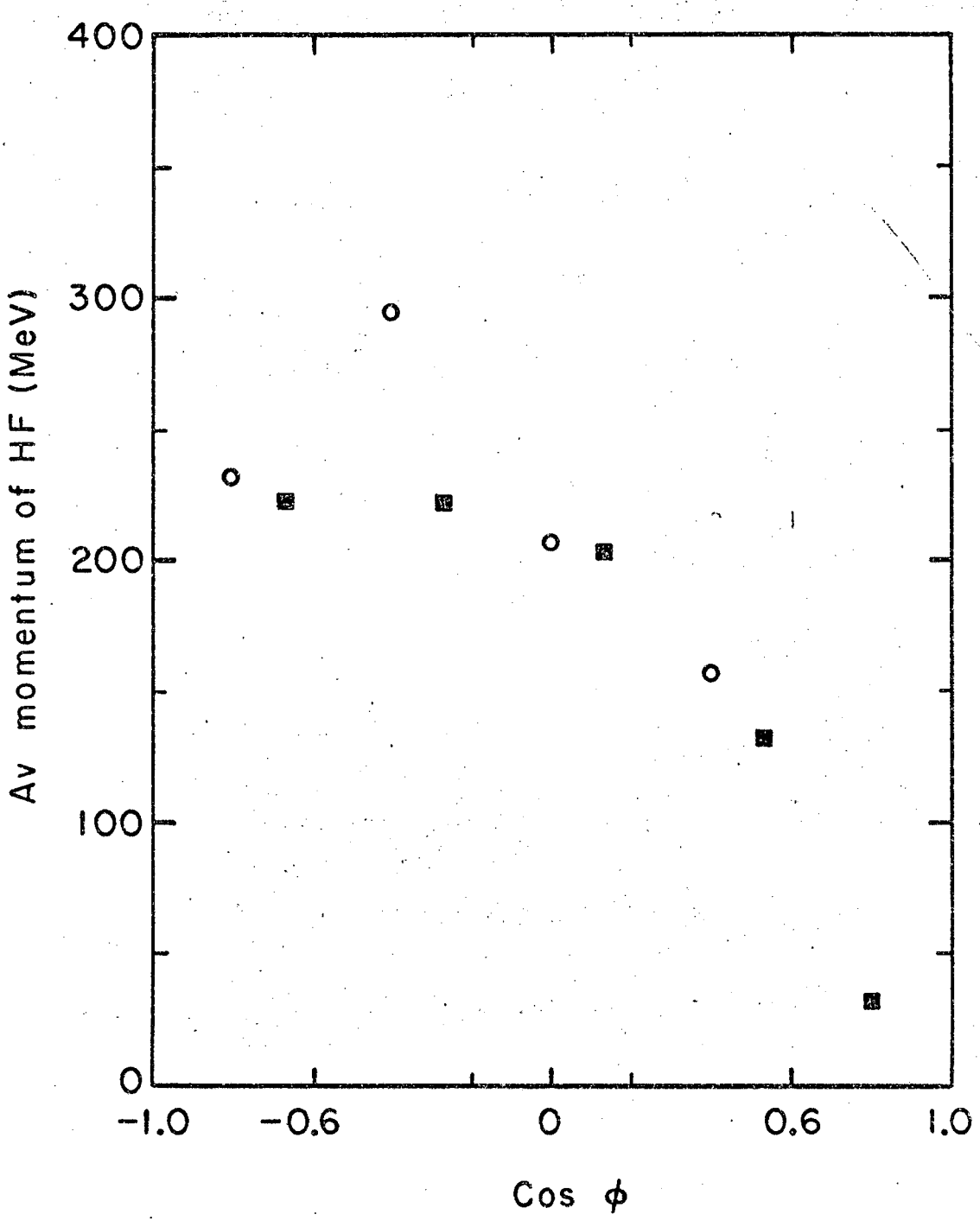


Fig. 9. Plot of cos φ (φ is the space angle between the hyperfragment and the pion or fast proton) versus the average hyperfragment momentum. The momentum average is taken within a space angle interval of Δ cos φ = 0.4. o, pion ■, proton.

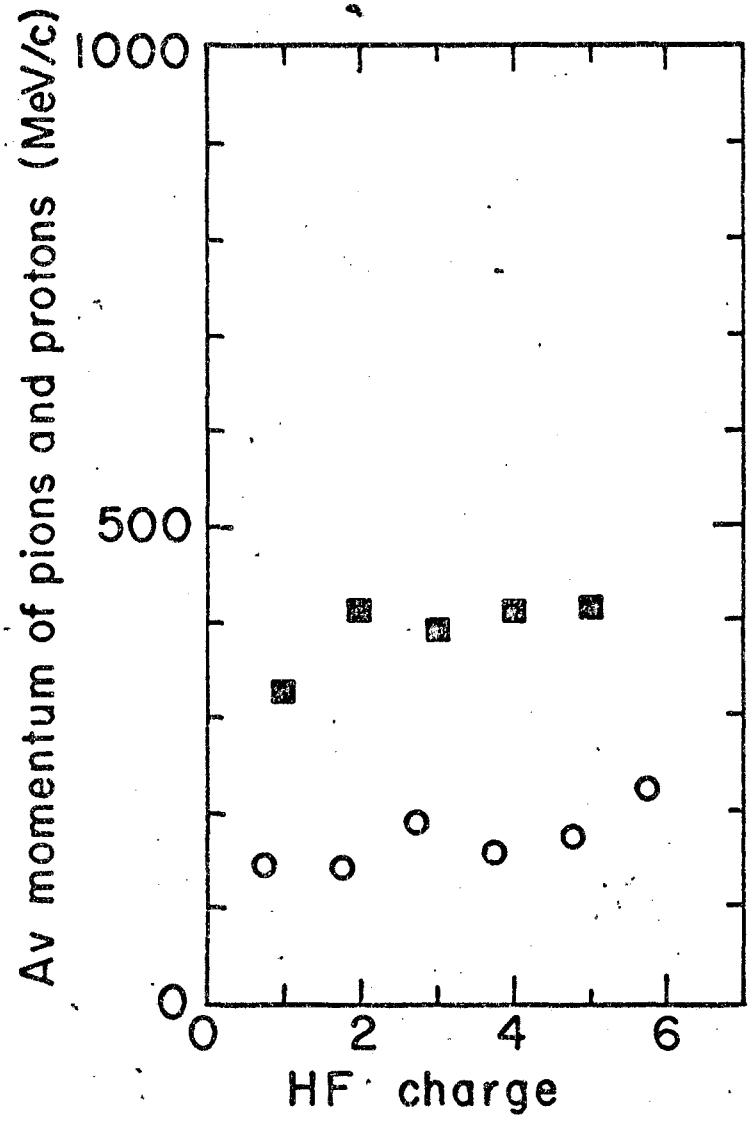


Fig. 10. Plot of average pion or proton momentum versus HF charge o, pion; ■ proton.

involving uncharged pions and sigmas will be dealt with in a later section.

Capture by a single nucleon (most of the energy is carried away by the π-meson):

$$K^- + N \rightarrow \Lambda + \pi \quad \text{(Direct } \Lambda \text{ production)} \qquad (1a)$$

$$K^- + N \rightarrow \Sigma + \pi \quad (\Sigma \text{ conversion, } \Sigma + N \rightarrow \Lambda + N). \qquad (1b)$$

Capture by two nucleons:

$$K^- + 2N \rightarrow \Lambda + N \text{ (Direct } \Lambda \text{ production)} \qquad (2a)$$

$$K^- + 2N \rightarrow \Sigma + N \ (\Sigma \text{ conversion, } \Sigma + N \rightarrow \Lambda + N). \qquad (2b)$$

Another conceivable reaction is $K^- + 2N \rightarrow \Lambda + N + \pi$. If a $\Sigma$ is produced initially, it may produce a $\Lambda$ in a secondary reaction with a nucleon. It was mentioned in Section 2 that the total number of selected hyperfragments was 63; of these, 19 events were accompanied by only high-energy protons ($T_p > 30$ MeV), 35 events were accompanied by charged pions, and 9 events by a pion and high-energy proton. Out of the total of 44 pions, 28 were brought to rest in the stack. The ratio of negatively charged stopping pions (22) to positively charged ones (6) was $\approx 4{:}1$ ($\pi^-/\pi^+$). The energies of the 16 pions not brought to rest were determined by ionization measurements. Eleven pions in this group had energies greater than 95 MeV and were presumably negative. Of the remaining five pions, one scattered inelastically but came to rest and its charge was found to be negative. A second pion was abosrbed in flight by a nucleus (DIF) but was so nearly stopped that we presumed it was negative in order for it to have penetrated the Coulomb barrier. This means that a maximum of only three pions could have been positive. If one assigns these three pions

of undetermined charge to the positive and negative groups in the same ratio (22:6) as the 28 stopping pions, then the $\pi^-/\pi^+$ ratio becomes 37/7 = 5.3. The energy spectra of all the pions is shown in Figure 11 (a) and (b).

6.1 One-Nucleon Capture

The one-nucleon interaction is discussed first. The single-nucleon interactions of $K^-$-mesons result in the production of a hyperon and a $\pi$-meson. The kinetic energies of all pions emitted from the hyper-fragment-parent stars have been plotted in Figure 11 (a) and (b). If charge exchange and charged-pion absorption are neglected,[10] then presumably all single-nucleon capture processes are included in Figure 11 (a) and (b) excepting those events in which neutral $\pi$-mesons are produced. The latter will be accounted for, however. The energy spectrum of the $\pi^-$ consists of two energy groups, the one large group centered around 70 MeV and a second smaller group centered around 125 MeV. Events with energies less than 100 MeV are assumed to consist largely of pions produced in reaction (1b) ($\Sigma$ conversion), since severe $\pi^-$ energy degradation by scattering within the nucleus is not probable as shown at the end of this section. All pions with energies greater than 90 MeV are presumed to be due to reaction (1a) (Direct $\Lambda$ production) with Q value $\approx$ 170 MeV.

For a positive pion, the only production mechanism other than charge exchange (considered negligible) is the reaction yielding $(\Sigma^-,\pi^+)$, with a Q value of 95 MeV. Thus there should be no pions above 90 MeV from the fraction in which any $\Sigma$-hyperon is involved.

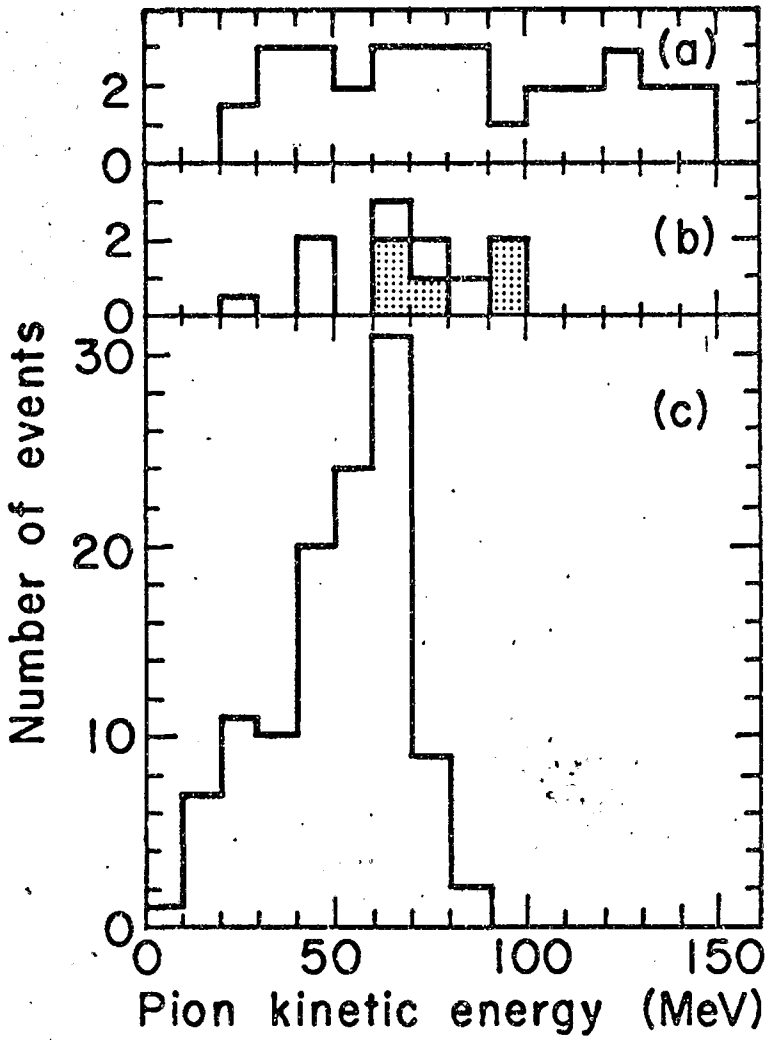


Fig. 11. (a) Energy spectrum of negative pions with dip angle $< 30^{o}$ emitted by HF parent stars. Events in the interval 0 to 30 MeV are normalized because here all angles were accepted. This explains the presence of a fraction of an event in the histogram. Full line, $\pi^-$. (b) Same as part (a) except positive pions and those of undetermined charge are represented. ■ $\pi^-$, ▨ $\pi^+$. (c) Energy spectrum of pions with dip angle $< 30^{o}$ emitted from $K^-$-capture stars and associated with $\Sigma^{\pm}$ (According to Dyer[57]). The data are not normalized: full line, $\pi$ (+,-,±).

In fact, none of the six positive pions observed had an energy greater than 81 MeV. Figure 11 (c) shows the energy distribution of pions produced in the one-nucleon reaction[57] $(\Sigma^{\pm},\pi^{\pm})$, in agreement with the above statements.

One can estimate the number of neutral pions emitted on the basis of the branching ratios obtained in the present work for $K^-$-meson absorption at rest in nuclear emulsion.

From Fig. 11 (b) is obtained the number of positive pions emitted. Pions of energy greater than 30 MeV were restricted by the criterion to those that had relatively flat trajectories (dip angle $\leq 30^{\circ}$). Therefore only half of the pions were measured and a correction factor of 2 must be introduced. Also, the number of pions of undetermined charge with energy less than 100 MeV were divided into positive and negative groups according to the procedure outlined in the preceding subsection. This added one pion to the $\pi^+$ group.

The total corrected number of positive pions that were presumably from the reaction $K^- + p \rightarrow \Sigma^- + \pi^+$ was 14, assuming 15 percent absorption[42]. This number of positive pions (14) then allows the calculation, on the basis of charge independence and the results of the present work, of the number of pions to be expected from each of the other single-nucleon reactions in which a $\Lambda$ might finally be produced, either directly or by $\Sigma$-conversion. These reactions are presented in Table XV.

TABLE XV

Single-nucleon channels with calculated and experimental branching-ratio results.

| | Interaction Channel | Number of Events Calculated | Experimental |
|---|---|---|---|
| (3) | $K^- + p \rightarrow \Sigma^+ + \pi^-$ | 29 | 28 |
| (4) | $K^- + p \rightarrow \Sigma^o + \pi^o$ | 17 | -- |
| (5) | $K^- + p \rightarrow \Lambda + \pi^o$ | 11 | -- |
| (6) | $K^- + n \rightarrow \Sigma^- + \pi^o$ | 10 | -- |
| (7) | $K^- + n \rightarrow \Sigma^o + \pi^-$ | 10 | -- |
| (8) | $K^- + n \rightarrow \Lambda + \pi^-$ | 25 | 26 |

For reaction (8) the calculated number 25 may be compared with the number found experimentally. There were 11 pions with energy greater than 100 MeV; these are attributed to reaction (8). The geometric (dip) factor increases this number to 22, and the correction for absorption brings the number up to 26 (we assumed 15 percent absorption as previously stated). Therefore, to reaction (8) is assigned the corrected experimental value of 26 pions. The calculated value was 25. This would indicate that the number of $\pi^-$-mesons from direct $\Lambda$ production, which scatter inelastically into the region of $T_\pi < 100$ MeV, is negligible. Hence the $\pi^-$ below 100 MeV were regarded as due primarily to $\Sigma$-conversion.

6.1.1. Direct $\Lambda$-production. Charged pions above 100 MeV energy comprise about $22/109 \approx 20$ percent of the total number of charged pions, and are produced in about $9/63 \approx 14$ percent of the light-hyperfragment-forming events. These are attributed to the direct $(\Lambda, \pi^-)$ reaction (1a).

This is a lower limit, to be sure. The total number of hyperfragments produced directly by this reaction could be somewhat larger owing to the greater inelastic-scattering cross-section for pions in this energy interval. As a result, there would be pions which, although they were produced by $(\Lambda,\pi^-)$ reactions, would scatter inelastically in the nucleus and thus be observed in the interval of energy range $T_\pi < 100$ MeV. As shown previously, it is likely that this number is not great. Inelastic scattering, however, may contribute to a degradation in energy of pions that were directly produced in association with $\Lambda$'s. Their $T_\pi$ usually remains above 100 MeV, however. There is also some loss of $\pi^-$-mesons, which are absorbed while coming out of the nuclei in which they are produced. The $\pi^-$ absorption loss is considered to be 15 percent.[42,58] Therefore, from charge independence and the results of this work one can estimate the total fraction of light hyperfragments formed by the capture of directly-produced $\Lambda$-hyperons from reaction (1a) together with those from the uncharged reaction $K^- + p \rightarrow \Lambda + \pi^0$, as not exceeding 20 percent.

6.1.2 Indirect production through $\Sigma$-conversion. In subsection 6.1.1 it was estimated that in 20 percent of the cases of light hyperfragment production from $K^-$-one-nucleon interactions, the $\Lambda$ is produced directly. Thus in the remaining 80 percent of the cases of one-nucleon capture, the $\Lambda$ forming the hyperfragment is presumably produced through the $\Sigma$-conversion reaction (1b), where an energetic nucleon is produced along with the $\pi$-meson. Thus, $\Sigma$-conversion in the capturing nucleus plays a major role in producing hyperfragments.

By comparing these results with data gathered by the Bologna

group[59] on inelastic scattering of π-mesons, one sees that high-energy protons are not produced from the inelastic scattering of π-mesons of average energy 50 MeV coming from the (Σ,π) reaction. The conversion processes involving Σ-hyperons are:

$$\Sigma^- + p \rightarrow \Lambda + n, \qquad (9)$$

$$\Sigma^+ + n \rightarrow \Lambda + p, \qquad (10)$$

$$\Sigma^o + p \rightarrow \Lambda + p, \qquad (11)$$

$$\Sigma^o + n \rightarrow \Lambda + n, \qquad (12)$$

From the above interactions one may deduce that a fast proton can be produced only through the absorption of a $\Sigma^+$ or $\Sigma^o$. However, the production of $\Sigma^+$ and $\Sigma^o$ must take place in association with a $\pi^-$ or $\pi^o$-meson. Therefore the interaction of the Σ-hyperon would be expected to have a strong correlation with negative π-mesons. If a hyperfragment-parent star emits both a high-energy proton and a charged pion, then the pion should generally be negative, and the concomitant fast proton may be regarded as an indicator of indirect Λ production by $\Sigma^+$ or $\Sigma^o$ absorption; $\Sigma^-$ absorption does not usually yield fast protons.[10]

Of the eight pions of identified sign associated with high-energy protons, only one was positive, thus indicating that most such protons originate from $\Sigma^+$ or $\Sigma^o$.

One may further compare our pion-energy spectrum in Figure 11 (a) with results of deuterium experiments[60] for which two distinct peaks correspond to direct Λ production and to indirect Λ (Σ-conversion) processes. The two peaks of this distribution are shifted towards values higher than those of our pion-energy spectrum. One could explain this difference by considering the deuteron structure to be

so loose that the absorption of a $K^-$-meson takes place on a more or less free nucleon, whereas in a complex nucleus this available energy is reduced by the higher binding energy of the nucleons. Furthermore one may compare the higher energy distribution of charged mesons emitted in direct Λ-production.[61] The two energy spectra are in agreement.

From the one-nucleon reaction followed by Σ-conversion, one expects in general that the energy of fast protons will be less than 60 MeV. The Fermi motion of the nucleons, however, complicates the picture. It has been calculated that in about 25 percent of the absorption cases the energy of the fast protons may be greater than 60 MeV.[62] This calculation is based on the assumption that the yield of fast protons in $\Sigma^o$ capture is half that of $\Sigma^+$ absorption. From the experimental data one gets about $2/9 \approx 22$ percent protons with $T_p > 60$ MeV from one-nucleon reactions (as identified by pion production). This is not in disagreement with the calculated value.

One may compare this minimum value of the ratio

$$\frac{\pi^- \text{ from direct } \Lambda^o}{\text{all HF pions}} = \frac{26}{82} = 0.32$$

with the corresponding ratio 0.31 deduced from the results of the deuterium experiment.[60] As a check one compares the ratio given by Cester et. al.[61], which also is 0.31.

6.2 Discussion of two-nucleon Capture

The simple two-nucleon reactions are given in the first part of Sect. 6. The energy distribution of fast protons produced with

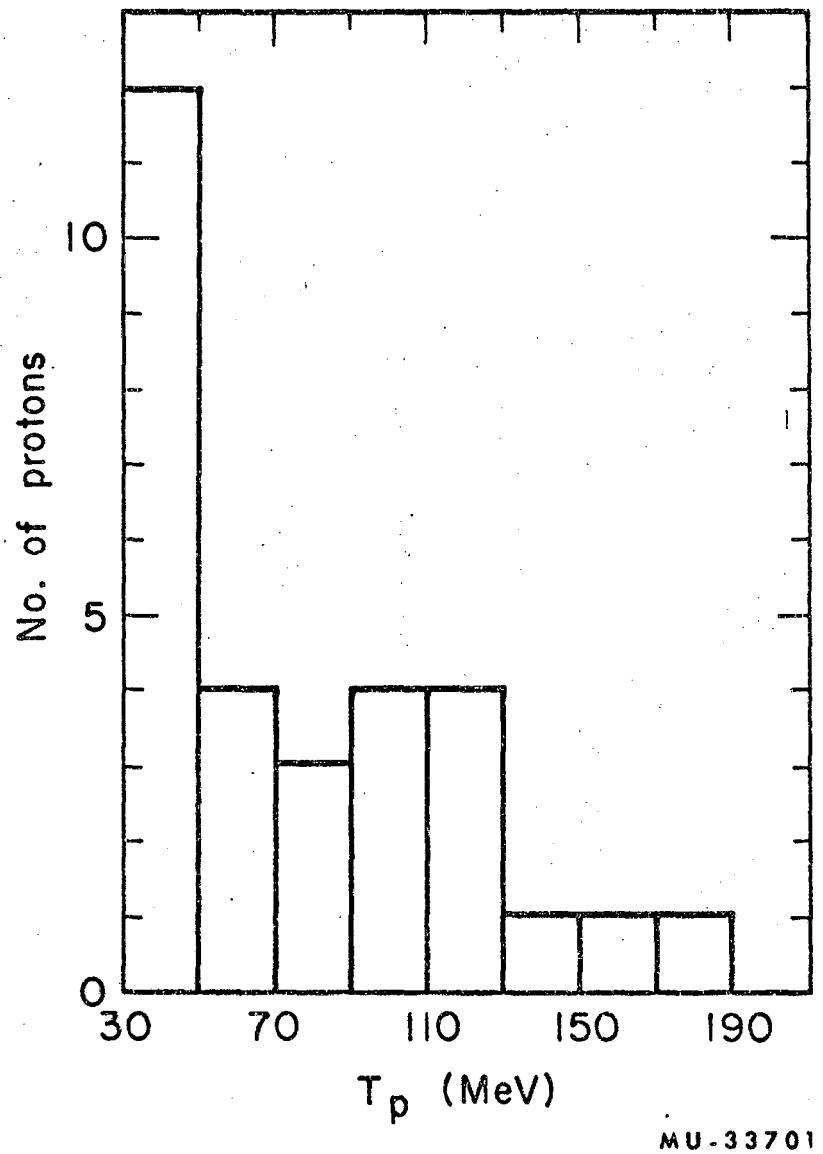


Fig. 12. Energy spectrum of fast protons with dip angle < 30° emitted by HF parent stars. The evaporation cutoff for protons is at 30 MeV.

hyperfragments in both the one-nucleon and two-nucleon reaction of $K^-$-mesons in emulsion nuclei are shown in Fig. 12. The cutoff for proton-evaporation prongs ($T_p < 30$ MeV) is also shown in this histogram. The interpretation of the histogram involves those processes in nuclear matter that contribute protons of energy > 30 MeV, e.g. (a) $\pi$-meson scattering or absorption, (b) $\Sigma^{+,o}$ absorption, and (c) two-nucleon interactions.

Events with only charged pions and no high-energy proton ($T_p > 30$ MeV) are probably produced in one-nucleon reactions. However, the stars having both a pion and a proton ($T_p > 30$ MeV) also may be produced through one-nucleon reactions according to Eqs. (1a) and (1b). The events without pions are not all due to the two-nucleon capture process, however. Such events may be from one-nucleon captures for which there was subsequent absorption of the pion or the emission of a $\pi^o$-meson. In subsection 6.1.1 it was mentioned that for most one-nucleon reactions the energy of the proton is < 60 MeV. Thus, one may certainly say that events with $T_p \geq 80$ MeV are due to multinucleon capture processes. Most of the protons from the multinucleon interaction should have energies in this region. Some 12 out of 19 events with protons alone, have energies $T_p > 80$ MeV. One may assume that these were produced in multinucleon reactions. Certainly one may estimate that 19/63 = 30 percent is an upper limit for the number of light hyperfragments originating in those multinucleon channels producing a fast proton secondary. Studies made of the branching ratios and reaction end-products for the multinucleon channels have led to the conclusion

that approximately 56 percent of the end products will consist of hyperon plus fast proton, while 44 percent will consist of hyperon plus fast neutron.[10,13] The neutron spectra are not expected to differ greatly from those of the proton. One may then deduce that if no more than 19 of the 63 HF events which produce fast protons are from the multinucleon channels (the other HF events possess pion secondaries, and are presumed to arise in single-nucleon interactions), then the same or smaller limit likewise exists for a similar sample of 63 HF events emitting fast neutrons, if one were able to obtain such a sample. Percentage-wise, therefore, the upper limit on light HF's produced in the multinucleon channels would not change: 19 fast protons plus 19 fast neutrons from a sample of 126 light HF events. This resulting limit is in agreement with the 30 percent figure for both light and heavy HF's obtained by Sacton.[14]

These multinucleon events could have been produced either through direct $\Lambda$-production or through the $\Sigma$-conversion process given in Equation (2b). There was one star in which two fast protons were produced. Both protons had energy $T_p > 80$ MeV. We may possibly explain their production through the $\Sigma$-conversion process, i.e., $K^- + p + p \rightarrow \Sigma^o + p$ and $\Sigma^o + p \rightarrow \Lambda + p$. In the final state there is $\Lambda + p + p$. Another possible explanation for $(\Lambda,2p)$ production is through a one-nucleon interaction in which $(\Lambda,2p)$ are produced in the final state through both pion absorption and $\Sigma$-$\Lambda$ conversion.

Of the events having a $\pi^+$-meson, only one had a pion with $T^\pi > 75$ MeV; its energy was 81 MeV. This is in agreement with previous results; the frequency of the two-nucleon (multinucleon) reaction pro-

ducing an energetic $\pi^+$-meson (i.e., $K^- + 2p \rightarrow \Lambda + n + \pi^+$) is small compared with the $\pi^+$-producing nucleon reaction given by Equation (1a).

As mentioned in the Section 6 discussion of $K^-$-capture by light and by heavy nuclei, in some of the hyperfragment events, $K^-$-absorption apparently took place in heavy elements (Ag,Br). Two of these 12 events belonged to the two-nucleon absorption reaction leading to hyperfragment production, as identified by fast protons ($T_p > 80$ MeV). This result is in agreement with the work of Condo and Hill[34], which indicates that a relatively small percentage of the multinucleon absorption takes place in heavy elements. It is consistent with the recent experimental results of a multinucleon yield of only 1 percent in deuterium[59] but of 17 percent in helium.[35]

## V. ROLE OF RESONANCE FORMATION IN $K^-$-INTERACTIONS

A study of the reaction channels of $K^-$-mesons interacting in complex nuclei would be incomplete without some attention being given to the role played by the formation of resonances, extremely short-lived states of association of two or more particles. The data on resonances or possible resonances produced by $K^-$-interactions in hydrogen, deuterium, and helium bubble chambers has been summarized in reference 63. The production by $K^-$ at rest in emulsion of one of these resonances, the $Y_o^*$ (1405), has been the subject of a paper[64] co-authored by the writer, and by A. Barbaro-Galtieri and F. M. Smith, published in Physics Letters, and in part reproduced here.

A T = 0 $\Sigma\pi$ resonant state at 1405 MeV, $Y_o^*$ (1405) has been observed in various bubble chamber experiments.[65,67] In nuclear emulsion, Esienberg et. al.[68] found that the $\Sigma\pi$ effective mass distribution showed a strong enhancement around 1405 MeV; Frisk and Ekspong[69] reported a peak in the p distribution ($p = p_\Sigma + p_\pi$) at a value corresponding to a mass of 1405 MeV in the $\Sigma\pi$ system produced in $C^{12}$ in the reaction $K^- + C^{12} \rightarrow \Sigma^\pm + \pi^\mp + B^{11}$. The latter researchers have recently redone their experiment under more favorable conditions and have published results[70] at variance with their original ones, but which confirm those of this work. All experiments have analyzed the interactions produced by $K^-$ at rest.

The bubble chamber experiments of Alexander et. al.[66] and Alston et. al.[67] yield a full width at half maximum of $\Gamma = 35 \pm 5$ and $\Gamma = 50$ MeV, respectively. Frisk and Ekspong,[69] in their original

experiment, seemed to observe a width of ≈ 1 MeV. The reason for this disagreement could be found in the fact that the two techniques have different resolution in energy. In our experiment, two large stacks of emulsion were used where the energy resolution is ≈ 1 MeV. The $\Sigma\pi$ mass spectrum obtained for $K^-$-interaction in $C^{12}$ shows prominent enhancement in the region around 1412 MeV. However, using an impulse model to calculate the expected distribution for direct $\Sigma\pi$ production, the observed results can be explained without appeal to $Y_o^*$ (1405) production. The 1 MeV width for the $Y_o^*$ (1405) resonance is not confirmed.

As mentioned in Chapter I, two large emulsion stacks were exposed to the $K^-$-beam from the bevatron. The $K^-$'s were brought to rest in the central part of the stacks and a large percentage of secondary particles came to rest in the emulsion. A sample of 270 events that showed $\Sigma\pi$ production has been analyzed. The criteria in selecting this sample were: (a) the $K^-$ interacted at rest, (b) the $\pi$ came to rest in the stack, and (c) if the $\Sigma$ decayed in flight, the secondary stopped in the stack. With these criteria the events not used were those where the $\pi$-mesons were either steep or else flat and left the stack or interacted in flight. These criteria do not introduce any bias because for $K^-$ at rest the distribution of prongs is expected to be isotropic. Eight measurements of each dip angle were made. All angles and all $\Sigma$-ranges have been measured by at least two people. The pion ranges were measured once. For all the steep tracks, distortion measurements have been made to correct the dip and projected angles, but this correction did not change the angle between

the $\Sigma$ and the $\pi$ by more than 0.5 deg. Suitable programs for the IBM 650 calculated for each event the total momentum ($\underline{p} = \underline{p}_\Sigma + \underline{p}_\pi$), the invariant mass of the $\Sigma\pi$ system M[$M^2 = (E_\pi + E_\Sigma)^2 - (\underline{p}_\Sigma + \underline{p}_\pi)^2$] and the appropriate errors. The average error in p was 1.9 MeV/c and never exceeded 3.5 MeV/c. The average error in M was 1.0 MeV and $(\Delta M)_{max}$ was 1.9 MeV.

Of the 270 events analyzed, 32 had additional prongs with a length shorter than that for a 30 MeV proton, which is the limit for evaporation prongs. This small sample of events with more than 2 prongs has been measured only for comparison. An attempt has been made to select from the two-prong events those in which the K-capture was on $C^{12}$. This selection is merely based on the possibility of detecting the recoiling nucleus, which is often difficult. The events have been divided into 4 categories based upon the appearance of the star center, i.e. those showing (a) recoil, (b) blob(s), (c) electron(s) and (d) clean star center. In Fig. 13(a) the recoil events are plotted on a scatter diagram with $M^2$ (square of the invariant mass of the $\Sigma\pi$ system) and $p^2$ (total momentum squared) as coordinates. In Fig. 13(b) the remaining events are plotted together using different symbols for the three categories. The straight lines are kinematical relations between $p^2$ and $M^2$ for different nuclei.[71] The selection criteria are the following:

(a) For each event the dip and projected angle of the recoil have been calculated from the relation $\underline{p} = -(\underline{p}_\Sigma + \underline{p}_\pi)$; also from p the length was calculated by assuming the $B^{11}$ mass for the recoil and using the range-energy relation of Heckman et. al.[56] All the

events were then checked under high magnification for agreement with the calculated quantities. Those recoil events with projected angles within $10^{o}$ of the calculated values and dip angles of the right order of magnitude were accepted if the recoil lengths were in agreement with the calculated ones. The expected lengths are $L \leq 5\mu$. Since the mean diameter of a grain in K.5 emulsions is $0.5\mu$, one does not expect the recoil criteria to be faultless for recoils with $L < 0.8\mu$ (2 grains) which corresponds to $p = 100$ MeV/c. For $p < 60$ MeV/c and a large calculated dip angle the recoil is not expected to have a detectable range, therefore such events with a clean star center have been accepted. Six of these events were added to the recoil sample. This a posteriori method of selecting the recoil events has been adopted in order to have a bias-free sample. In fact, it is often difficult to decide whether there is a recoil, a blob, or an electron, especially for length $< 1.5\mu$. On the other hand, the probability for an electron to have the same length and direction expected for the recoil of a given event is small.

(b) Included in the category of blob events were those with more than one grain at the star center of those with a single grain not satisfying the calculated recoil criteria; Part of the events on $O^{16}$ or heavy nuclei are included in this category, because they have shorter recoils than expected for $B^{11}$.

(c) The electron events were those with recognizable slow electrons or those with 2 or 3 grains which were directional but did not satisfy the criteria for recoils. This category may contain

events on $O^{16}$, for which the recoil direction is the same as for $C^{12}$, but whose length is shorter.

(d) The clean events were those with no visible electron, recoil or blob and with a $p > 60$ MeV/c. Satisfying these criteria were only 16 events out of 218 with $p > 60$ MeV/c. This means that one expects only 1.4 events with $p > 60$ MeV/c to be in this category rather than among the recoils.

Table XVI summarizes the separation of events into different categories

TABLE XVI Number and Type of Events Analyzed

| Type | Recoil | Blobs | Electrons | Clean | > 2 prongs | Total |
|---|---|---|---|---|---|---|
| Number of Events | 133 | 43 | 45 | 17 | 32 | 270 |

In Fig. 13 one notes the following:

(1) The recoil events lie between the line for $O^{16}$ and the line corresponding to the last excited state for $B^{11}$ (for which the excitation energy is enough to give $B^{11} \rightarrow Li^{7} + \alpha$). In this sample, it may be expected confidently that the majority of the reactions are on $C^{12}$. In fact the $N^{15}$ range-energy relation is appreciably different from that of $B^{11}$ for $p > 100$ MeV/c. There doubtless remains some $O^{16}$ contamination, especially at low momenta, but its effect on the given interpretation of the process under study is negligible.

(2) The > 2 prong events lie far from the solid lines in Fig. 13(b). These interactions are those in which a heavy nucleus has been left in an excited state and the excitation energy was enough to allow an

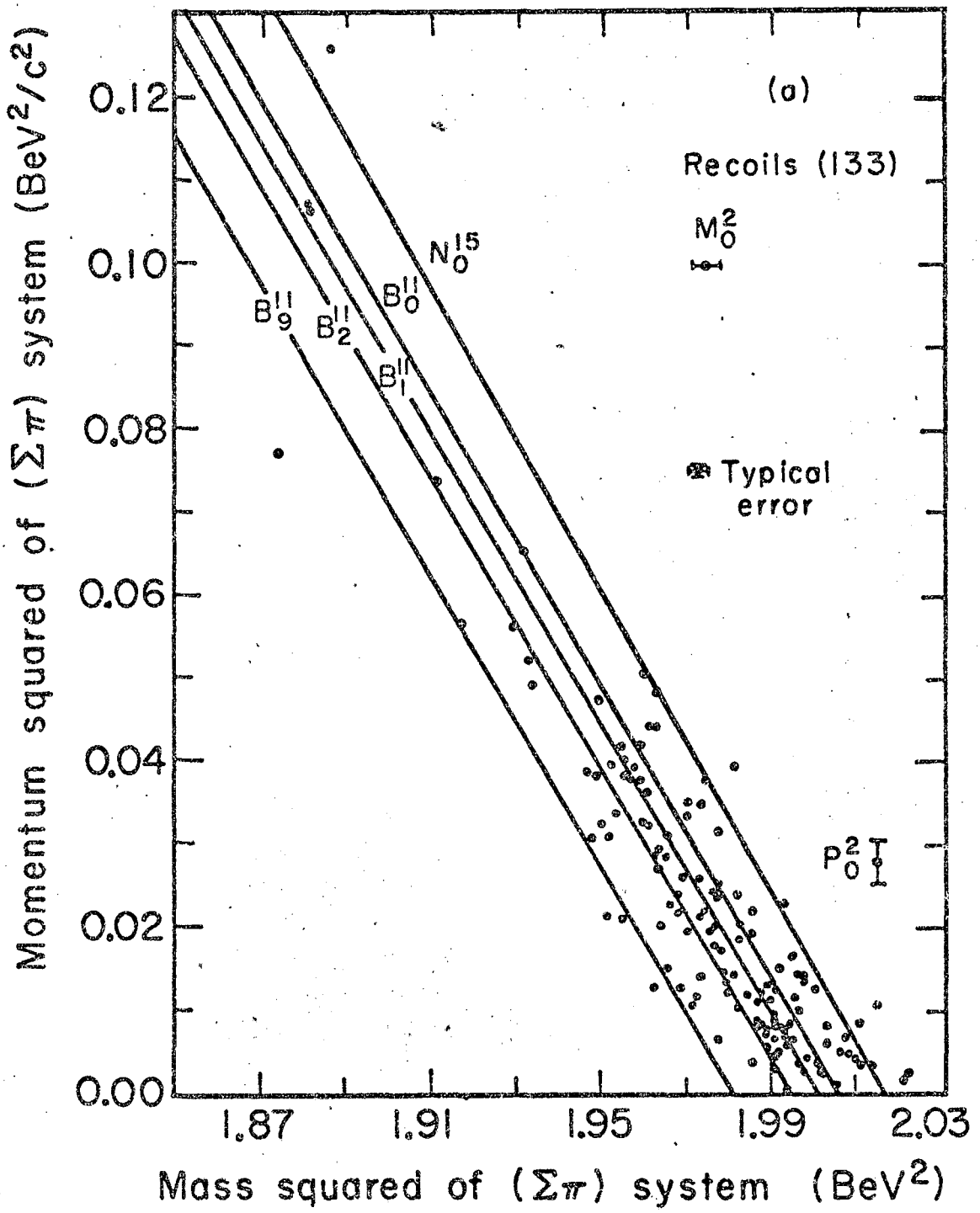


Fig. 13a. Scatter diagram of $M^2$ versus $p^2$; (a) recoil events. The solid lines represent kinematical relations for several kinds of nuclei. The symbol ⟷ indicates the $M^2$ and $p^2$ values for $Y_0^*$ of M = 1405 ± 1 MeV produced in $C^{12}$ and with $B^{11}$ in its ground state. The number of events is given in parentheses.

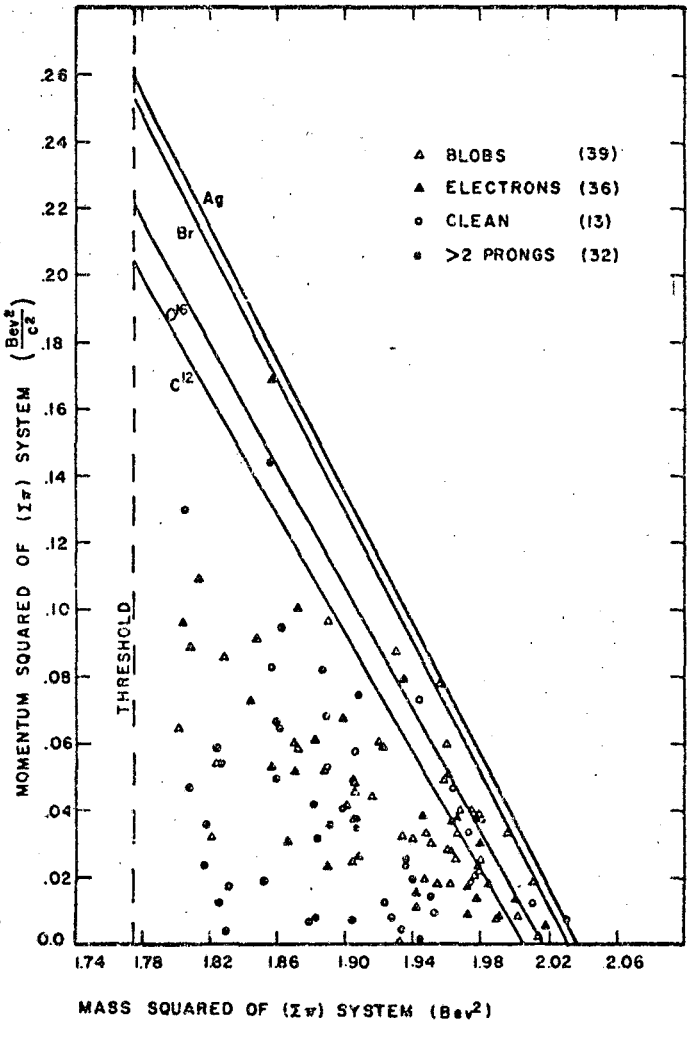


Fig. 13b. Scatter diagram of $M^2$ versus $p^2$; (b) blob, electron or clean events and events with more than 2 prongs. The solid lines represent kinematical relations for several kinds of nuclei. The symbol ⊢—o—⊣ indicates the $M^2$ and $p^2$ values for $Y_o^*$ of M = 1405 ± 1 MeV produced in $C^{12}$ and with $B^{11}$ in its ground state. The number of events is given in parentheses.

evaporation prong, or those in which the $\pi$ or the $\Sigma$ had a secondary interaction on a proton. Heavy nuclei are most likely to give such events because of the large density of nucleons.

(3) Some 70 percent of the blob, electron, or clean events lie near the solid lines in Fig. 13(b). Many of them are probably interactions on $O^{16}$ (from the way they have been selected). The remaining 30 percent show a distribution similar to that of the > 2 prong events.

In the following the analysis is restricted to the recoil events only. In Fig. 13(a) the mass 1405 MeV area does not show any particular enhancement; a peak seems to occur at 1412 MeV. It is evident that the $B^{11}$ is often left in an excited state; indeed, the distribution of points indicates excited states are preferred. From the diagram this means that for $Y_o^*$ production in $C^{12}$ one does not expect a peak in the $p^2$ distribution because different excited states give different $p^2$ values corresponding to a 1405 MeV invariant mass ($M^2 = 1.974$ GeV$^2$). Since the position of the peak observed by Frisk and Ekspong in their original experiment is at p = 170 MeV/c, all their events would correspond to $Y_o^*$ production in the $B^{11}$ ground state. In Fig. 14 the momentum distributions are plotted (a) for all our sample of 2-prong events and (b) for the 133 interactions on $C^{12}$. The distributions do not present any evidence of peaking at any particular p value.

It is very important to include among the interactions on $C^{12}$ those events with $p < 100$ MeV/c.

There may be contamination from interactions on $O^{16}$, but if such events had not been taken the M distribution would have had a non-negligible bias. In Fig. 15 is plotted the M distributions for

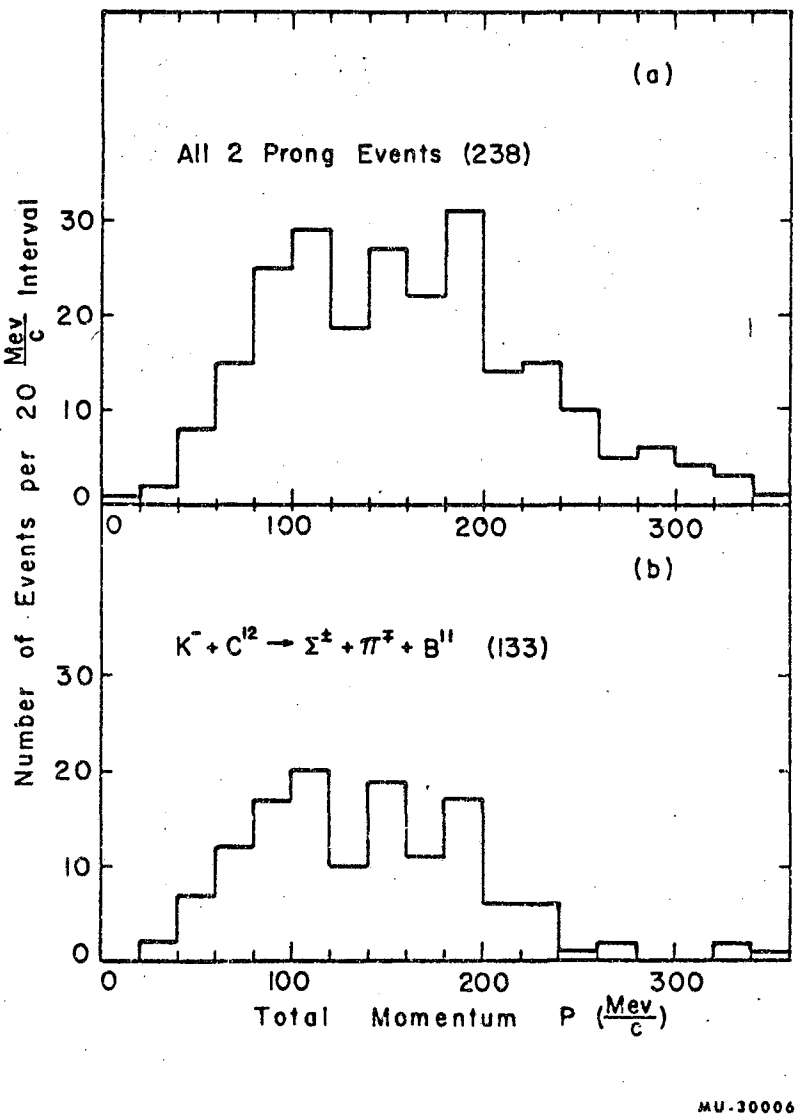


Fig. 14. $P = P_{\Sigma} + P_{\pi}$ distribution; (a) all 2-prong events, and (b) recoil events, that is $\Sigma\pi$ production on $C^{12}$. Co-authors F. M. Smith and A. Galtieri will shortly publish an article treating bias in the part of the spectrum below 120 MeV/c.

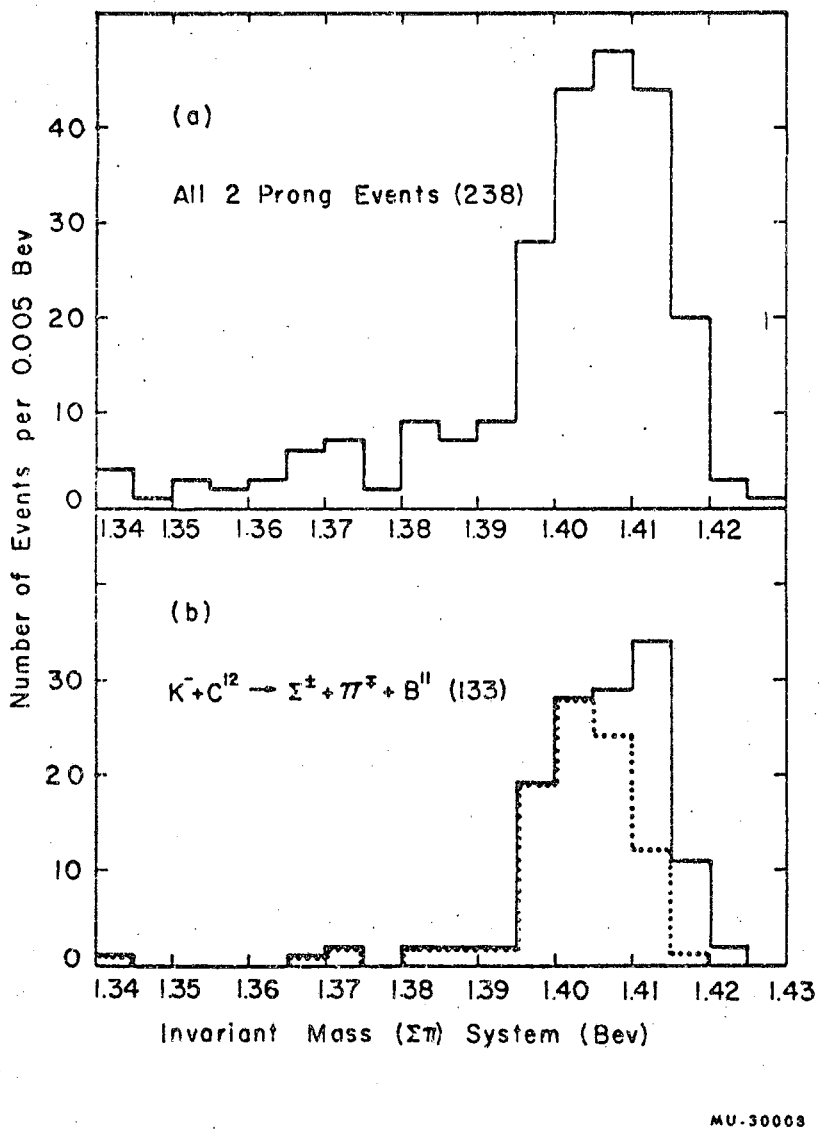


Fig. 15. Mass of ($\Sigma\pi$) system distribution, (a) all 2-prong events and (b) $\Sigma\pi$ production on $C^{12}$. In (b) the dotted distribution is obtained using only events with $p > 100$ MeV/c.

(a) all the 2-prong events and (b) the interactions on $C^{12}$. In the latter the dotted-line distribution represents the distribution we would have if there had not been taken any events with $p < 100$ MeV/c. As one can see in this case there is a symmetrical distribution around 1405 MeV which could easily simulate a resonance. The M distribution in Fig. 15 does not differ substantially from the one observed by Eisenberg et. al.[68] This distribution can easily be interpreted as that expected for direct $\Sigma\pi$ production.

An impulse model, as suggested by Block,[72] has been calculated for the reaction

$$K^- + C^{12} \rightarrow \Sigma^{\pm} + \pi^{\mp} + B^{11}. \qquad (1)$$

It assumes that the capture takes place on a single nucleon and neglects final-state interactions. It has been calculated for $K^-$ captures in s, p and d states. The wave function for the nuclear density distribution in $C^{12}$ was assumed to be the same as the charge distribution measured by Hofstadter.[73] This calculation has been done for $K^-$-captures such that the $B^{11}$ has been left in its ground state, and the data can be compared with the impulse model only for a restricted sample of events. In Fig. 13(a) the $B_1^{11}$ line ($B^{11}$ in its first excited state) lies apart from the $B_o^{11}$ line (the ground state for the $B^{11}$ nucleus) by only a distance corresponding to 1.5 standard deviations, where it is assumed for $\sigma$ the average error on the events. For this reason it is hard to select a sample of events to compare with the impulse model. It was assumed that the events within 1.5 $\sigma$ from the $B_o^{11}$ line are of type (1). In Fig. 16 the $M^2$ and $p^2$ distributions of these 39 events are compared with the calculated distributions. An s-state

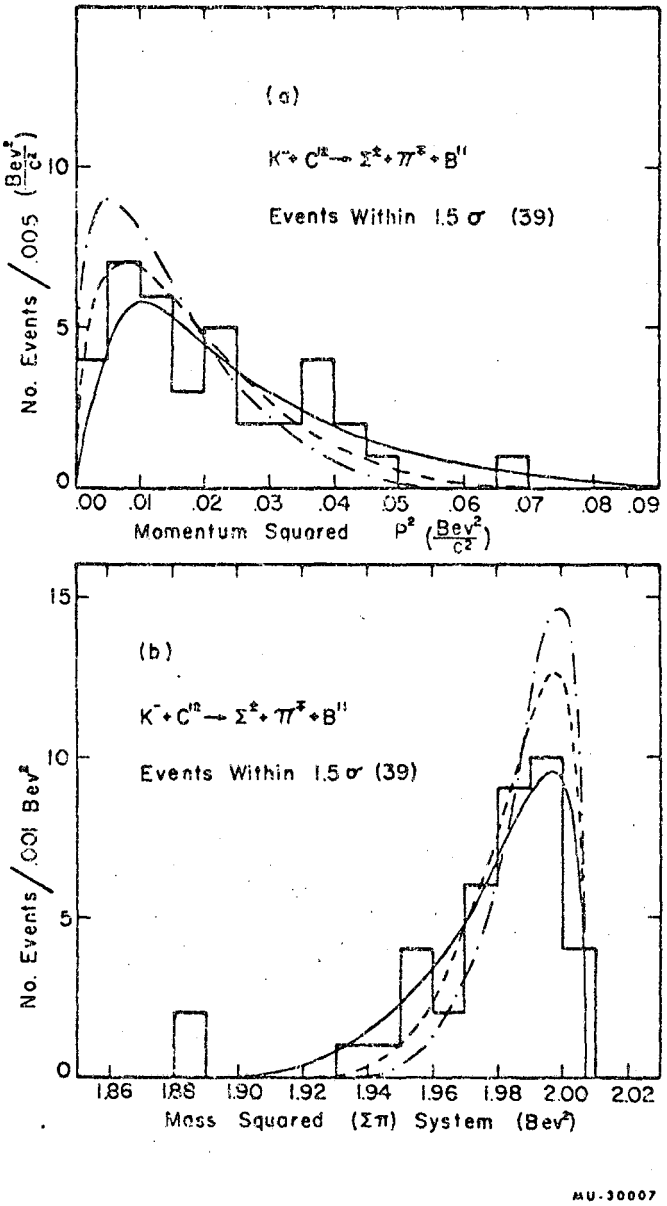


Fig. 16. (a). $p^2$ distribution of the events within 1.5 standard deviations from the $C^{12}$ line in Fig. 1a. These are assumed to be events for which $B^{11}$ has been left in its ground state. (b) $M^2$ distribution of the same sample. The curves are calculated by an impulse model: ——— s-state capture, ---- p-state capture (using $\psi_{21}$), -.-.-.- d-state capture (using $\psi_{32}$).

capture seems to give a better fit than the others, but the statistics are too poor to allow any conclusion in this matter. In any case it is evident that one can explain the data without any appeal to $Y_o^*$ (1405) production. The distributions of all the events on $C^{12}$ (Figs. 14(b) and 15(b)) could be easily obtained by a superposition of curves calculated for different excited states of $B^{11}$, thus shifting the $M^2$ peak to lower values.

In conclusion, the data do not show any evidence for $Y_o^*$ production in $C^{12}$ with a width of 1 MeV. If the $Y_o^*$ (1405) had a width of $\Gamma = 1$ MeV it would travel a distance $d \approx 23$ fm before decaying. Since the $B^{11}$ radius is $\approx 2.5$ fm, the $\Sigma$ and $\pi$ should not have interactions inside the nucleus. Therefore with the given energy resolution one should detect its production. If the $Y_o^*$ (1405) has a 40 MeV width one would be able to see such a width in the distribution in Fig. 15(b). Moreover, it would only go about 1 fm before decaying. The width would then be further increased by Coulomb scattering and secondary interactions within the nucleus. Because both excited and ground states are involved, the reaction is not well defined. Consequently, in this experiment one cannot distinguish production of $Y_o^*$ with a width of about 20 MeV from nonresonant direct production. If the width is of this order of magnitude, one cannot measure it in any case because the mass distribution will be broadened for the above reasons.

## VI. DISCUSSIONS AND CONCLUSIONS

In the present work the branching ratios have been determined for the single-nucleon reaction channels of the $K^-$-interaction at rest with complex nuclei of research emulsion. These values are in general agreement with those obtained by the European Collaboration[10] from fewer events.

The ratio of the number of negative pions to the number of positive pions emitted from $K^-$-interaction stars has been found for various pion energy intervals. These results indicate that the ratio is not constant but decreases with increasing energy. For the pion kinetic energy between 0 and 30 MeV, the value is $4.9 \pm 0.9$. For the next interval, 30 to 60 MeV, this work yields $3.4 \pm 0.6$, while for the interval 60 to 90 MeV the result is $3.3 \pm 0.7$. The ratios found by the European Collaboration[10] are $3.8 \pm 0.8$, $4.0 \pm 0.9$, and $4.0 \pm 1.6$ respectively. However, their statistics are successively poorer the greater the energy of the interval. In fact they were unable to determine the charge of any pions of energy beyond 90 MeV, while 11 such events were identified in this experiment.

A determination of the relative number of captures on light and on heavy nuclei was made for both the single-nucleon and the multi-nucleon reaction channels.

Use was made of the presence of prongs of short range L, where $2.5\ \mu < L < 30\ \mu$, and of Auger electrons. It was found that the pion emission frequency for $K^-$-captures at rest was close to the same order of magnitude for both light and heavy nuclei (1.16:1.0) with a

slightly greater frequency for the C, N, O events.

On the other hand, the $K^-$-interaction with a light nucleus is 2.36 times as likely to produce a fast hyperon as is a $K^-$-interaction with a heavy nucleus.

The hyperfragment production mechanism has been investigated by studying the spectra of accompanying pions. For the single-nucleon channel it is found that a majority ($\geq$ 80 percent) of the light hypernuclei which emerge from the interaction star originate in $\Sigma$-conversion processes. Analysis of the accompanying fast proton spectra ($T_p > 30$ MeV) was made in order to determine the extent of the role played by the multinucleon reaction. It was found that at most 30 percent of the light hypernuclei originated in multinucleon reactions. An attempt was made to separate $K^-$-captures in C, N, or O from those in Ag or Br using the same criteria listed previously. Only a small percentage ($\leq$ 20 percent) of the production of these light hyperfragments was found to take place in the heavy elements.

The role played by resonance formation in $K^-$-interactions in complex nuclei has been investigated. In particular the evidence for the $Y_o^*$ (1405) production has been studied by analyzing the $\Sigma\pi$ mass spectrum obtained for $K^-$-interaction in $C^{12}$. Although the $\Sigma\pi$ mass spectrum shows enhancement in the region around 1412 MeV, this can be explained using an impulse model and without recourse to any $Y_o^*$ (1405) production. The energy resolution with the present emulsion stacks is 1 MeV. Therefore, the production of a resonance with a width at half-maximum of 1 MeV, as was reported by one group[69], should have been

detected. In fact, a resonance half-width of up to 20 MeV would be apparent, but such is not the case. The results of the present work do not show evidence for $Y_o^*$ (1405) production in $C^{12}$ with a width of 1 MeV.

## VII. ACKNOWLEDGMENTS

I am exceedingly grateful to Professor Walter H. Barkas for his guidance and understanding, for his kindness and consideration, and especially for his monumental patience and tact in leading a very green graduate student through the requirements of the Ph.D. program. He has taught me all that I know of experimental physics.

My thanks are also due to the physicists of the Barkas group who have helped me at one time or another: Harry Heckman, John Dyer, Zack Osborne, Francis Smith, and particularly David Young and Douglas Greiner.

I express appreciation to the many scanners and technicians of the Barkas group, including Carl Cole, Tom Coen, James Downing, Tom Traut, Larry Goldstein and others too numerous to mention, who have completed many tasks in connection with this work. Two scanners should be singled out and commended for their performance of a variety of measurements and calculations: Ernestine Beleal and Thelma Giolli.

I acknowledge with sincere appreciation the secretarial help of Carol Pierson, Pam Rambeau, and especially the precision, yeoman service done by Janice Dickson .

Finally, I am indebted to those friends and relations who have continued to encourage me in the completing of this work, now finished. Deo gratias.

This work was done under the auspices of the U. S. Atomic Energy Commission.

## Appendix I. Scattering cross section formulas for $K^-$-nucleon processes

We present here the cross sections for the various $K^-$-nucleon processes: elastic scattering, charge exchange scattering, and absorption. The derivations of these formulas were carried out in References 16 and 19. The $K^-$ + p elastic scattering cross section is

$$\sigma_{el} = \pi \left| \frac{A_o}{1-ikA_o} + \frac{A_1}{1-ikA_1} \right|^2 , \qquad (1)$$

while the $K^-$ + p charge exchange scattering cross section is

$$\sigma_{c.e.} = \pi \left| \frac{A_o}{1-ikA_o} - \frac{A_1}{1-ikA_1} \right|^2 . \qquad (2)$$

The $K^-$ + p absorption cross section is

$$\sigma_{abs} = \frac{2\pi}{k} \left[ \frac{b_o}{|1-ikA_o|^2} + \frac{b_1}{|1-ikA_1|^2} \right] . \qquad (3)$$

The $K^-$ + n cross sections are simpler because only T = 1 plays a role. The elastic scattering cross section is

$$\sigma_{el} = \pi \left| \frac{A_1}{1-ikA_1} \right|^2 , \qquad (4)$$

while the charge exchange scattering cross section is

$$\sigma_{c.e.} = \pi \left[ \frac{A_1}{1-ikA_1} \right]^2 , \qquad (5)$$

and the absorption cross section is

$$\sigma_{abs} = \frac{2\pi}{k}\left[\frac{b_1}{|1-ikA_1|^2}\right] . \qquad (6)$$

When a more sophisticated treatment is done, and Coulomb and mass difference effects are considered, then the following expressions result [16]

$$\frac{d\sigma_{el}}{d\Omega} = \left| \frac{\mathrm{cosec}^2\frac{\theta}{2}}{2Bk^2} \exp\left\{\frac{2i}{kB}\ln\sin\frac{\theta}{2}\right\} + \frac{C}{2D}\left\{A_o(1-ik_oA_1) + A_1(1-ik_oA_o)\right\}\right|^2 , \qquad (7)$$

$$\sigma_{c.e.} = \frac{\pi k_o C^2}{k}\left|\frac{A_o - A_1}{D}\right|^2 , \qquad (8)$$

$$\sigma_{abs} = \frac{2\pi C^2}{k}\left\{b_o\left|\frac{1 - ik_oA_1}{D}\right|^2 + b_1\left|\frac{1 - ik_o A_o}{D}\right|^2\right\} . \qquad (9)$$

here B is the Bohr radius of the $K^-$ + p system, and C is the Coulomb penetration factor $\frac{2\pi}{kB}[1-\exp(-\frac{2\pi}{kB})]^{-1}$. The relative momentum of the $\bar{K}^oN$ system is $k_o\hbar$, and D is a quantity which takes account of the mass difference. The expression for D reduces to $(1-ikA_o)(1-ikA_1)$ for $k = k_o$.

## Appendix II. Details of the Emulsion Stack Exposure

The first emulsion stack employed in this experiment, the A-stack, consisted of 216 pellicles of Ilford K.5 emulsion, each one measuring 6 inches × 9 inches in area and 600μ in thickness. The pellicles were assembled and milled following the regular procedure used by the Barkas group at LRL and outlined in Reference 25. The assembled stack was exposed to the bevatron's 450 MeV/c $K^-$ beam separated by the coaxial velocity spectrometer.[26] Grid printing of the stack with the Berkeley grid was according to the methods mentioned in Reference 25. The results of the analysis of particle density and distributions in the A-stack were reported by Dyer.[27]

The second stack utilized was the C-stack, a 9-inch cube of emulsion consisting of 320 Ilford K.5 pellicles, assembled and milled in the same manner as the A-stack. The exposure of this stack took place at three separate times. In the first test run on November 1, 1960, the negative K-meson beam (with momentum 760 MeV/c) from the Murray coaxial velocity spectrometer, was incident on a copper absorber immediately in front of the C-stack. This absorber had a mass of 119.280 $g/cm^2$, calculated to be sufficient to stop the beam in the interior of the stack which was kept at a temperature between 0 and $4^\circ$ C during the bevatron exposure in order to reduce fading of the latent image and to hamper the growth of fog. Approximately 31,000 negative K-mesons were accumulated during the first exposure lasting 52 hours. On November 16, a second exposure of the C-stack was begun under similar conditions and lasted 9 hours. The momentum of the negative K-particles

was only 600 MeV/c this time; the beam came into the stack from the direction opposite to that of the first exposure. Now, however, the absorber consisted of two parts: The first was copper of mass absorption coefficient 83.014 $g/cm^2$ at the bubble chamber and the second was copper plus an aluminum container with total mass absorption coefficient 36.014 $g/cm^2$. This brought the beam to rest interior to the stack. Due to technical difficulties with the beam, the run was finally discontinued and the emulsion stack was removed to the storage mine on November 28, and kept there at dry ice temperature until the run resumed on March 9, 1961.

For the third and final exposure, the conditions were approximately the same as the previous two. The momentum of the negative K-beam was 750 MeV/c and the copper absorber used was of mass density 150.8 $g/cm^2$, while the aluminum refrigeration box had a mass density of 0.6 $g/cm^2$. The range to be traveled in emulsion was 4.5 inches, or half the distance through the C-stack, yielding a mass density of 151.2 $g/cm^2$. Thus the total absorber was 194.5 $g/cm^2$. After the conclusion of the exposure, the stack was grid printed with the Berkeley grid as referred to in References 25 and 28.

## Appendix III. Range Determinations by the Grid-Plot Method

The details of the printing of the Berkeley grid on the emulsion pellicle are contained in Reference 25. The pellicle alignment procedure is outlined in References 25 and 28.

The ranges of particles were estimated by referring to the grid system printed on the pellicles. A reconstruction of the track was made by plotting on graph paper the points at which the particle passes from one pellicle to another or where a scatter of more than $5^{\circ}$ takes place. When these points are connected by straight lines as in Figure III-1, with pellicle numbers alongside, then the "true" projected range of the particle is approximated by the series of straight lines. To convert this projected range to the space range of the particle, it is necessary to take account of the pellicle thickness corresponding to each straight line segment. The range may be calculated in this fashion by an application of the Theorem of Pythagoras. That is,

$$R = \sum_{i=1}^{N} \sqrt{L_i^2 + t_i^2}$$

where R is the total range of the particle in emulsion, L is the projected length of the track, measured in a single pellicle at most, and t is the total thickness of the pellicle traversed by the particle in completing the length L. Therefore, t is usually the original thickness of the pellicle, if the track passes through without any scatters of $5^{\circ}$ or more.

As a check[27] this method was applied to 13 pions whose ranges of

up to 8 centimeters had been determined by means of the range scope.[30] The difference between the two methods was less than 4 percent in all cases.

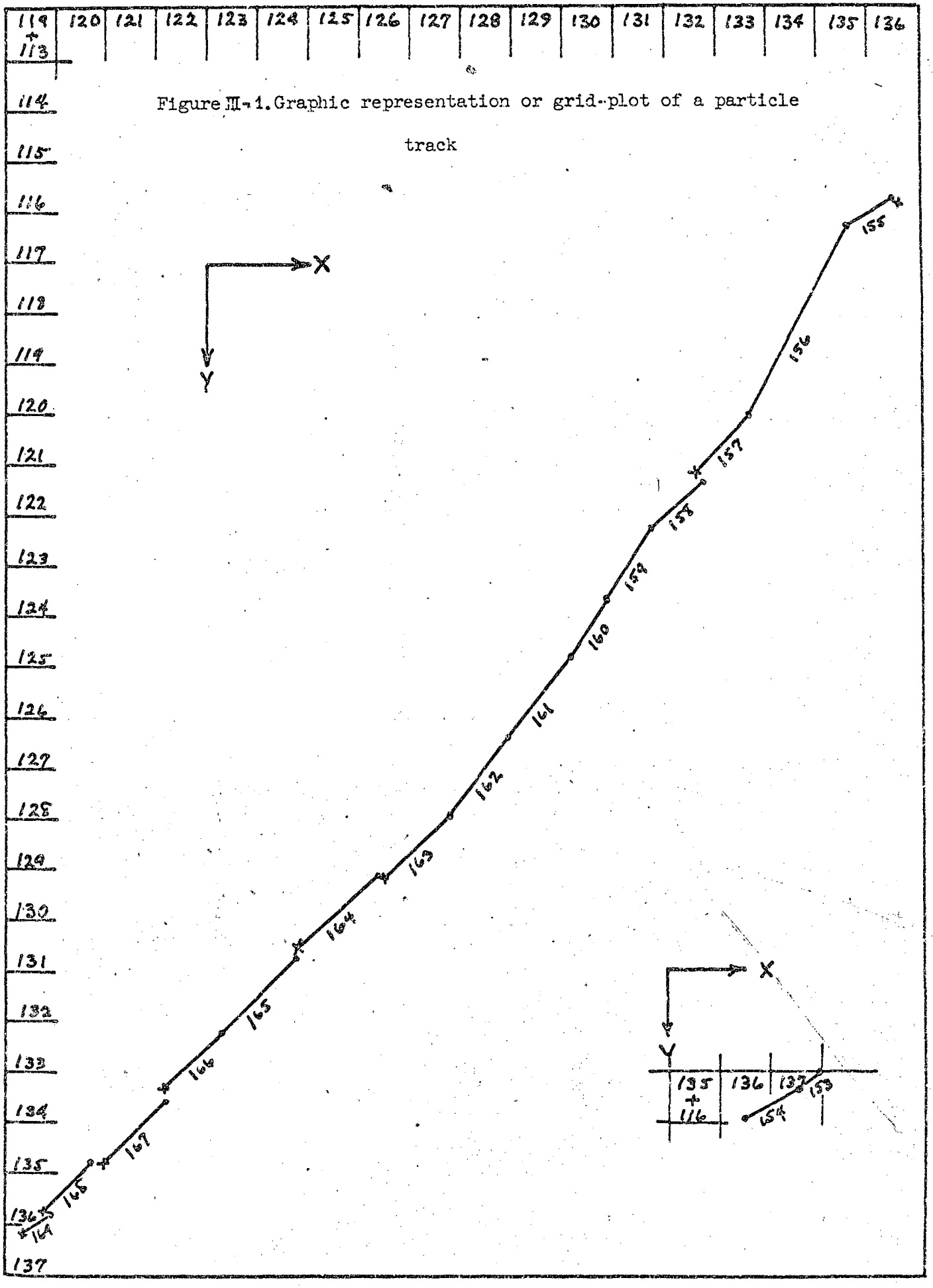


Figure III-1. Graphic representation or grid-plot of a particle track

## Appendix IV. Grain Density of Emulsion Tracks

The grain-density in the emulsion track of a charged particle is an indicator of its velocity. Measurements of the true grain-density have been made by several methods on the tracks of electrons, pions, K-mesons, protons, Σ-hyperons, and α-particles.[31] The curve of grain-density vs. velocity in K.5 emulsion has been obtained and is presented in Figure IV-1. The results found by different objective methods and by different observers were in agreement. It was found that, owing to the finite density of silver-halide crystals in the emulsion, the grain-density saturates. The nature of the saturation effect was studied. A decomposition of the grain-density into primary and secondary components was made. Even at the minimum of grain density, some 25 percent of the grains are of secondary origin. Since only primary grains are affected by the relativistic rise of the grain-density, the interpretation of the plateau/minimum grain-density ratio is affected. Special observations of the grain-density in the relativistic region were made, taking precautions to avoid temperature, fading, and development-difference effects. A rise to the plateau of 18 percent in the primary grain-density was found. This implies a mean excitation potential for AgBr of 442 ev. Finally, indices that measure emulsion quality were suggested: the maximum gap density, $B_{max}$ (related to the developed grain diameter $\alpha = 1/eB_{max}$); the grain density $g_{min}$, produced at the minimum of ionization; and the saturation lacunarity, $L_o$. These three quantities were defined operationally in Reference 31.

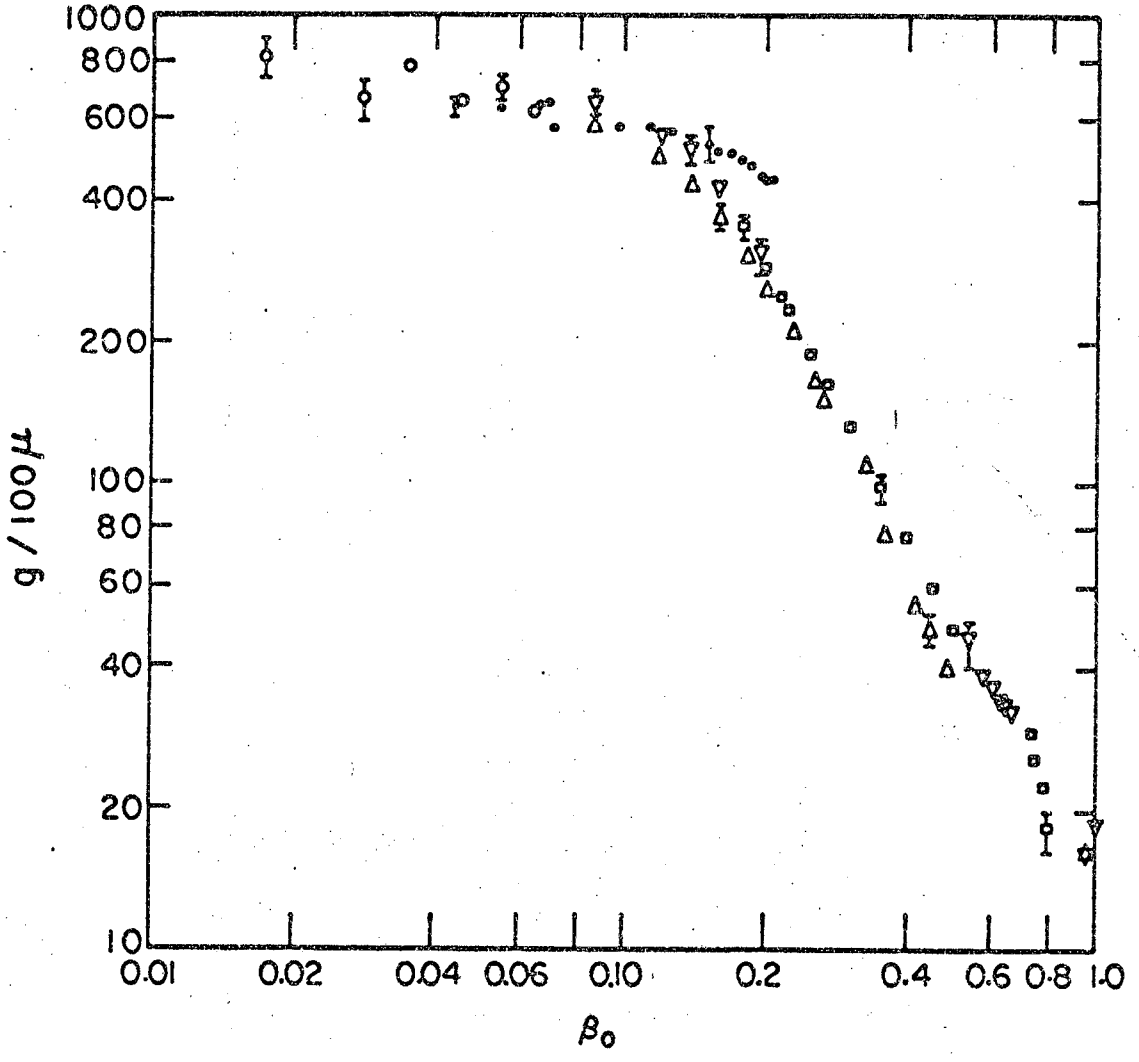


MU-23692

Fig.IV-1. The observed grain-density of singly and doubly-charged particles in Ilford K-5 emulsion vs. velocity β. Measurements by different methods were made in overlapping regions of β. The legend is * minimum in this K-5 emulsion; o tracks of Σ-hyperons (lacunarity method); Δ tracks of K-mesons, protons and π-mesons (lacunarity method); □ tracks of the same particles using the gap-length coefficient method, ∇ tracks of K-mesons, π-mesons and electrons (blob count method); and . tracks of α-particles (lacunarity method). Typical errors are indicated.

REFERENCES

1. P. Lal, Y. Pal, and B. Peters, Proc. Ind. Acad. of Sci, 38, 398 (1953).

2. Report of the Committee on K-Particles, Padua-Conference Suppl., Nuovo Cimento 12, 433 (1954).

3. J. Hornbostel and E. O. Salant, Phys. Rev. 93, 902 (1954).

4. J. Hornbostel and E. O. Salant, Phys. Rev. 98, 218 (1955).

5. W. H. Barkas, W. F. Dudziak, P. C. Giles, H. H. Heckman, F. W. Inman, C. J. Mason, N. A. Nichols, F. M. Smith, Results from an Enriched Negative K-Meson Beam, Lawrence Radiation Laboratory Report UCRL-3627, 1956, Phys. Rev. 105, 1417 (1957).

6. Joseph J. Murray, A Coaxial Static-Electromagnetic Velocity Spectrometer for High Energy Particles, Lawrence Radiation Laboratory Report 3492, May 1957.

7. Luis W. Alvarez, Berkeley Bubble Chamber, CERN Symposium (1956).

8. C. Franzinetti, and G. Morpurgo, Nuovo Cimento Suppl. 6, 469 (1957).

9. R. H. Dalitz, Reports on Progress in Physics 20, 163 (1957).

10. B. Bhomik, D. Evans, D. Falla, F. Dassen, A. A. Kamal, K.K. Nagpaul, D. J. Prowse, G. Alexander, R. H. W. Johnston, C. O'Ceallaigh, E. H. S. Burhop, D. H. Davis, R. C. Kumar, W. B. Lasich, M. A. Shaukat, F. R. Stannard, G. Bacchella, A. Bonetti, C. Dalworth, G. Occhialini, L. Scarsi, M. Grilli, L. Guerriero, L. Von Lindern, M. Merlin, and A. Saladin, Nuovo Cimento 13, 690 (1959); 14, 315 (1959). European Collaboration.

11. M. C. Amerighi, F. Baldassare, M. Beniston, A. Bonetti, D. H. Davis, M. DiCorato, C. Dilworth, E. Ferreira, E. Frota-Pessoa,

W. B. Lasich, N. Raina, M. Rene, J. Sacton, and A. C. Sichirollo, Nuovo Cimento, 12 91 (1959).

12. G. Morpurgo, Ann Rev of Nuc Science 11, 41 (1961).

13. E. H. S. Burhop, D. H. Davis, J. Zakrzewski, Prog Nucl Physics 9, 155 (1964).

14. J. Sacton, Thesis, University of Brussels.

15. M. Sakitt, T. B. Day, R. G. Glasser, N. Seeman, J. Friedman, W. E. Humphrey, R. R. Ross, Phys. Rev. 139, B719 (1965).

16. R. H. Dalitz, and S. F. Tuan, Annals of Physics 10, 307 (1960).

17. Y. Eisenberg, W. Koch, E. Lohrmann, M. Nikolic, and H. Winzeler, Nuovo Cimento 9, 745 (1958).

18. L. W. Alvarez, Report to the 9th International Conference on High Energy Physics (Kiev), UCRL-9354, August 1960.

19. R. H. Dalitz and S. F. Tuan, Annals. of Physics 8, 100 (1959).

20. W. E. Humphrey and R. R. Ross, Low-energy Interactions of $K^-$-Mesons in Hydrogen, UCRL 10018, Phys. Rev. 127, 1305 (1962).

21. M. B. Watson, M. Ferro-Luzzi, and R. D. Tripp, Phys. Rev. 131, 2248 (1963).

22. T. Akiba and R. H. Capps, Phys. Rev. Letters 8, 457 (1962).

23. O. Dahl, N. Horwitz, D. H. Miller, J. J. Murray, and M. Watson Proceedings of the Tenth International Conference on High Energy Physics, Rochester, N. Y. 1960 (Interscience Publishers, New York, 1960), p. 415.

24. R. L. Schult and R. H. Capps, Phys Rev. 122, 1659 (1961).

25. Walter H. Barkas, Nuclear Research Emulsions, (Academic Press

New York, 1963) Volume I, Chapter 4.

26. N. Horwitz, J. J. Murray, R. Ross, and R. Tripp, 450-MeV/c $K^-$ and $\bar{P}$ Beams at the Northwest Target Area of the Bevatron Separated by the Coaxial Velocity Spectromenter, UCRL 8269, June 1958.

27. J. N. Dyer, Analysis of the $K^-$-Beam Transmitted by Murray Spectrometer, UCRL-8364 Supplement, January 1959.

28. Walter H. Barkas, Equipment and Methods for Automatic Track Analysis, UCRL-8482, August 1958.

29. Walter H. Barkas, The Range-Energy Relation in Emulsion, Part 2: The Theoretical Range, UCRL-3769, April 1957.

30. C. J. Mason, and W. H. Barkas, A Microscope with Automatic Coordinate Readout Adapted for Calculating Particle Ranges, UCRL-8306, May 1958.

31. J. W. Patrick, and W. H. Barkas, The Grain-Density of Emulsion Tracks, Nuovo Cimento 23, N. 1 Supp., June 1961, LRL report UCRL-9692.

32. W. H. Barkas, Proceedings of the Third International Symposium on Nuclear Photography (Moscow) LRL report UCRL - 9180, June 1960.

33. The Cooke multiple scattering microscope is simply a commerical microscope mounted on a Cooke stage. It has provided results comparable to those obtained using the Koristka scattering microscope.

34. G. T. Condo, and R. D. Hill, Phys. Rev. 129, 388 (1963).

35. Helium Bubble Chamber Collaboration, $K^-$-Interactions at Rest in Helium, in Proceedings of the Tenth Annual Conference on High-

Energy Physics, Rochester, N. Y., 1960 (Interscience Publishers, New York, 1960).

36. D. H. Perkins, Phil. Mag. 40, 601 (1949).

37. M. G. K. Menon, H. Muirhead, and O. Hochat, Phil. Mag. 41, 584 (1950).

38. M. Demeur, A. Huleux, and G. Vanderhaeghe, Nuovo Cim. 4, 509, (1956).

39. C. Grote, I. Kundt, U. Krecker, K. Lanius, K. Lewen and H. W. Meier, Nuovo Cimento 14, 532 (1959).

40. G. Brown, and I. S. Hughes, Phil. Mag. 2, 777 (1957).

41. E. B. Chesik, and J. Schneps, Phys. Rev. 112, 1810 (1958).

42. G. Bernardini, and F. Levy, Phys. Rev. 84, 610 (1951).

43. D. Evans, B. D. Jones, Sonjeevaiah, J. Zakrzewski, M. J. Beniston, V. A. Bull, and D. H. Davis, Proceedings of the Royal Society (London), A, 262, 73 (1961).

44. M. Danysz and J. Pniewsky, Phil. Mag. 44 348, (1953).

45. W. F. Fry, Ann Rev Nucl Sci 8, 105 and references contained therein (1958).

46. R. Levi-Setti, W. E. Slater and V. L. Telegdi, Nuovo Cimento Suppl. 10, 68 (1958).

47. W. E. Slater, Nuovo Cim. Suppl. 10, 1 (1950).

48. E. M. Silverstein, Nuovo Cim, Suppl 10, 41 (1958).

49. D. Abeledo, L. Choy, R. Ammar, R. Levi-Setti, W. E. Slater, S. Limentani, P. E. Schlein, and P. H. Steinberg, Nuovo Cim. I, 15, 181 (1960); II, 19, 20 (1961); III, 22 1171 (1961).

50. F. W. Inman (Ph.D. Thesis), University of California Lawrence Radiation Laboratory Report UCRL-3815, June 1957 (unpublished).

51. M. Baldo-Ceolin, C. Dilworth, W. F. Fry, W. D. B. Greening, H. Huzita, S. Limentani, and A. E. Sichirollo, Nuovo Cim. 7, 328 (1958).

52. V. Gorge, W. Koch, W. Lindt, M. Mikolic, S. Subotic-Nikolic, and H. Winzeler, Nuclear Physics 21, 599 (1961).

53. R. H. Dalitz, Repts. Prog. Phys. 20, 163 (1957).

54. S. Iwao and E. C. G. Sudarshan, Phys. Rev. Letters 4, 140 (1960).

55. J. W. Patrick and P. L. Jain, Mechanism of Hyperfragment formation in $K^-$-Capture, Nuclear Physics 73, 681 (1965),LRL Report UCRL-11328 Rev. 1.

56. H. H. Heckman, B. L. Perkins, W. G. Simon, F. M. Smith, and W. H. Barkas, Phys Rev. 117, 544 (1960).

57. J. N. Dyer (Ph.D. Thesis), Lawrence Radiation Laboratory Report UCRL-9450, November 1960 (unpublished).

58. W. Koch, V. Eisenberg, M. Nikolic, M. Schneeberger and H. Winzeler, Helva Phys. Acta 33, 237 (1960).

59. Bologna-Munich-Parma and Turin Collaboration, $\Lambda$ Production and Decays, in Proceedings of Tenth Annual International Conference on High-Energy Physics, Rochester, N. Y., 1960 (Interscience Publishers, New York, 1960), p. 440

60. O. Dahl, N. Horwitz, D. H. Miller, J. J. Murray, and P. G. White, Phys. Rev. Letters 6, 142 (1961).

61. R. Cester, G. Ciochetti, A. Devenedetti, A. M. Cinesa, G. Rinado, C. Deney, K. Gottstein, and W. Puschel, Nuovo Cim. 22, 1069 (1961).

62. M. Nikolic, Y. Eisenberg, W. Koch, M. Schneeberger, and H. Winzeler, Helv. Physics Acta 33, 221 (1960).

63. A. H. Rosenfeld, A. Barbaro-Galtieri, W. H. Barkas, P. L. Bastien, J. Kirz, and M. Roosm, Data on Particles and Resonant States.

64. A. Barbaro-Galtieri, F. M. Smith, and J. W. Patrick, Physics Letters, 5, 63 (1963).

65. M. Alston, L. Alvarez, P. Eberhard, M. Good, W. Graziano, H. Ticho, S. Wojcicki, Phys. Rev. Letters 6, 698 (1961).

66. G. Alexander, G. R. Kalbfleisch, D. H. Miller and G. A. Smith, Phys. Rev. Letters 8, 447 (1962).

67. M. Alston, L. Alvarez, M. Ferro-Luzzi, A. Rosenfeld, H. Ticho and S. Wojcicki, Proceedings of the International Conference on High-Energy Physics, CERN 1962, p. 311.

68. Y. Eisenberg, G. Yekutieli, P. Abrahamson, and D. Kessler, Nuovo Cimento 21, 563 (1961); Aix-en-Provence Conf. Proc. I, 383 (1961).

69. A. Frisk and A. G. Ekspong, Physics Letters 3, 27, (1962).

70. P. J. Carlson, O. Danielsson, A. G. Ekspong and A. Frisk, Nuclear Physics 74, 642 (1965).

71. Actually they are calculated by applying energy-momentum conservation to the process $K^- + n \rightarrow \Sigma + \pi + n'$, where n and n' are nuclei in their ground states differing in atomic number by unity. Lines are shown only for C, O, Br and Ag which are the most frequent nuclei in emulsion. The nucleus n' is often left in an excited state and in that case the corresponding line

is shifted to the left. In Fig. 1a are shown lines for $B^{11}$ in some of the excited states; $B_9^{11}$ corresponds to that energy sufficient to allow $B^{11} \rightarrow Li^7 + \alpha$.

72. M. M. Block, Nuovo Cimento 20, 715 (1961).

73. R. Hofstadter, Revs. Modern Physics 28, 214 (1956).

This report was prepared as an account of Government sponsored work. Neither the United States, nor the Commission, nor any person acting on behalf of the Commission:

A. Makes any warranty or representation, expressed or implied, with respect to the accuracy, completeness, or usefulness of the information contained in this report, or that the use of any information, apparatus, method, or process disclosed in this report may not infringe privately owned rights; or

B. Assumes any liabilities with respect to the use of, or for damages resulting from the use of any information, apparatus, method, or process disclosed in this report.

As used in the above, "person acting on behalf of the Commission" includes any employee or contractor of the Commission, or employee of such contractor, to the extent that such employee or contractor of the Commission, or employee of such contractor prepares, disseminates, or provides access to, any information pursuant to his employment or contract with the Commission, or his employment with such contractor.